European Journal of Medicinal Chemistry 277 (2024) 116765

Contents lists available at ScienceDirect

European Journal of Medicinal Chemistry

journal homepage: www.elsevier.com/locate/ejmech

Research paper

Isoalantolactone/hydroxamic acid hybrids as potent dual STAT3/HDAC inhibitors and self-assembled nanoparticles for cancer therapy

Hualong Mo [a], JieYing Liu [a], Zhengxi Su [a], Deng-Gao Zhao [a,*], Yan-Yan Ma [a,**], Kun Zhang [a], Qi Wang [b], Chun Fu [b], Yao Wang [a], Meiwan Chen [c], Burong Hu [b,***]

[a] School of Pharmacy and Food Engineering, Wuyi University, Jiangmen, 529020, China
[b] Department of Radiation Medicine, School of Public Health and Management, Wenzhou Medical University, Wenzhou, 325035, China
[c] State Key Laboratory of Quality Research in Chinese Medicine, Institute of Chinese Medical Sciences, University of Macau, Macau, 999078, China

ARTICLE INFO

Handling Editor: Z Liu

Keywords:
HDAC
Self-assembled nanoparticles
STAT3
Isoalantolactone
Antitumor

ABSTRACT

Conventional chemotherapy, especially with natural anticancer drugs, usually suffers from poor bioavailability and low tumor accumulation. To address these limitations, we developed a novel approach for modifying natural products in which amphiphilic hydroxamic acid hybrids based on a natural product: isoalantolactone (IAL) were rationally designed. Compound **18** is identified as a highly potent dual signal transducer and activator of transcription 3 (STAT3)/histone deacetylases (HDAC) inhibitor and induces autophagy and apoptosis. **18** exhibits higher antitumor potency than IAL and the hydroxamic acid SAHA *in vitro* and *in vivo*. Furthermore, **18** self-assembled in water to form nanoparticles (**18** NPs), which facilitated the accumulation of drugs in tumor tissues and promoted their cellular uptake, resulting in superior anticancer efficacy compared to free **18**. Compared to drug-drug conjugates, hydroxamic acid hybrids have a smaller molecular weight and can synergize with various anticancer drugs. Overall, these findings indicate that **18** utilizing nanomedicines and dual-target drugs provide an efficient strategy for the rational design of dual-target drugs and the modification of natural products.

1. Introduction

Cancer has long been one of the leading cause of mortality worldwide [1]. Chemotherapy is essential for cancer treatment. Natural products are a sustainable source of anticancer drugs; more than 60 % of commercially available anticancer drugs originate from natural sources [2,3]. Natural anticancer drugs usually have several limitations, such as poor water solubility, nonspecific selectivity, severe multidrug resistance, and severe side effects. Hence, it is often necessary to modify the structures of natural products. However, the modification of natural products usually requires sophisticated synthesis [4].

Nanovehicles, including polymeric nanoparticles, liposomes, vesicles, and inorganic materials, have been developed as drug carriers to address these limitations [5–7]. However, the drug-loading capacity in a typical nanodrug delivery system is low, and many carriers may cause adverse reactions [8–10].

In recent years, a new concept of drug-drug conjugates has been proposed, in which hydrophilic drugs are directly conjugated to hydrophobic drugs to form a high-drug content nano delivery system without additional carriers [11–15]. In most drug-drug conjugates, two distinct pharmacophores/molecules are connected through a linker that does not exist in either of the two pharmacophores, and these conjugate molecules are much larger than conventional small-molecule drugs. In addition, relatively few types of medicines are available for the preparation of amphiphilic drug conjugates. Scientists aspire to maximize the degree of pharmacophore overlap using the merged pharmacophore mode to produce smaller and simpler molecules with favorable physicochemical properties [16,17]. Merged molecules that maximize pharmacophore overlap have higher ligand efficiency, smaller molecular weight, and better physical and chemical properties than drug–drug conjugates. We envisioned a promising drug self-delivery system in which the dual-target drug was designed in the merged-molecule mode with a small molecular weight similar to conventional drugs.

Histone deacetylases (HDACs) are major epigenetic factors that

* Corresponding author.
** Corresponding author.
*** Corresponding author.
E-mail addresses: zhaodenggao@wyu.edu.cn (D.-G. Zhao), j002293@wyu.edu.cn (Y.-Y. Ma), brhu@wmu.edu.cn (B. Hu).

https://doi.org/10.1016/j.ejmech.2024.116765
Received 3 June 2024; Received in revised form 2 August 2024; Accepted 9 August 2024
Available online 12 August 2024

modulate various cellular processes, including proliferation, apoptosis, metabolism, and immunogenicity [18,19]. HDAC inhibitors are recognized as "sensitizing drugs" that can synergize with various anticancer drugs. Typically, the classical HDACi pharmacophores contain a surface recognition group (cap), a linker, and a zinc-binding group (ZBG) [20,21]. The hydroxamic acid group is a well-known ZBG and is present in many HDACi. Several hydroxamic-acid-based hybrids have been reported in recent years designed using the merged pharmacophore mode [22–26]. However, self-assembled hydroxamic acid-based hybrids have not yet been reported.

The signal transducer and activator of transcription 3 (STAT3) is crucial for the survival, invasion, and growth of human cancer cells. Recent studies have demonstrated that the inhibition of HDACs increases histone acetylation at the leukemia inhibitory factor receptor (LIFR) gene promoter, which activates JAK1-STAT3 signaling and restrains the antitumor effect of HDACi in solid tumors [27]. Therefore, suppressing STAT3 could potentially increase the sensitivity of solid cancers to HDACi [28].

In this work, we designed a series of STAT3/HDAC dual-target inhibitors based on amphiphilic isoalantolactone/hydroxamic acid hybrids. The amphiphilic hydroxamic acid hybrids comprise a flexible linker, a hydrophilic hydroxamic acid moiety, and a hydrophobic isoalantolactone unit that serves as a "cap" (Scheme 1). Isoalantolactone (IAL), an active sesquiterpene lactone naturally present in many medicinal plants, was recently identified as a STAT3 inhibitor [29,30]. The prepared IAL hydroxamic acid hybrids exhibited various favorable properties: (1) Owing to their amphiphilic properties, the hydroxamic acid-IAL hybrids can yield self-assembled nanoparticles in water that can be easily internalized by tumor cells via the enhanced permeability and retention effect. (2) Hydroxamic acid-IAL hybrids targeting STAT3 and HDAC exhibited a synergistic anticancer effect and achieved a better antitumor effect than HDACi alone. (3) Hybrid molecules have smaller molecular weights and better physical and chemical properties than drug-drug conjugates.

2. Results and discussion

2.1. Synthesis and screening of hybrid molecules

The hybrid molecules were designed as shown in Schemes 2 and 3. Previous studies have demonstrated that amino acids can be used as the linker in the development of dual HDAC inhitor [31]. Thus, we introduced different amino acids to connect *ortho*-aminoamide and IAL, and compounds **1**–**11** were synthesized (Scheme 2). For HDACs, HDAC1、HDAC2、HDAC3 and HDAC6 were selected as they represent two distinct classes of HDACs family. HDAC inhibitors SAHA and Chidamide were chosen as positive controls. As presented in Table 1, in the HDACs activity test, the *o*-aminobenzamide derivatives exhibit poor activity against HDACs. The HDACs inhibitor activity of the compounds with R configuration is superior to that of the compounds with S configuration, as the R substitution has a lower binding energy with the HDACs protein. In comparison to their unsubstituted counterparts (**1**), R-substitutions enhances activity and the order of activity is methyl > isobutyl > benzyl > ethyl > tertbutyl substitutions, which could be attributed to the fact that the compounds with bulky substituents cannot effectively combine with the HDACs protein, thereby presenting poor HDACs inhibitory activity. Among the *o*-aminobenzamide derivatives, compound **2** displayed the best inhibitory activity against HDACs, indicating that the (R)-CH_3 group on the linker is crucial.

Subsequently, N-hydroxybenzamide was replaced by hydroxamic acid, and compounds **12**–**14** were prepared (Scheme 3). The HDAC inhibitory activities of compounds **12**–**14** were superior to those of compounds **1**–**11**, because the hydroxamic acid group can chelate well with the zinc ion in the HDACs active center and form hydrogen bonds with the surrounding residues. Compared with their unsubstituted counterparts (**12**), hydroxamic acid derivatives **13** and **14** with methyl-substitutions showed decreased activity.

Eventually, N-hydroxycinnamamide was used as the ZBG group, resulting in the synthesis of compounds **15**–**19**. The HDAC inhibitory activities of compounds **15**–**19** were better than those of compounds **12**–**14**, which might be explained by the fact that N-hydroxycinnamamide can better conjugate with the phenylalanine residues in the active center of HDAC. The comparison among the 3-subtituted N-hydroxycinnamamide derivatives **15**–**17** demonstrated that the CH_3

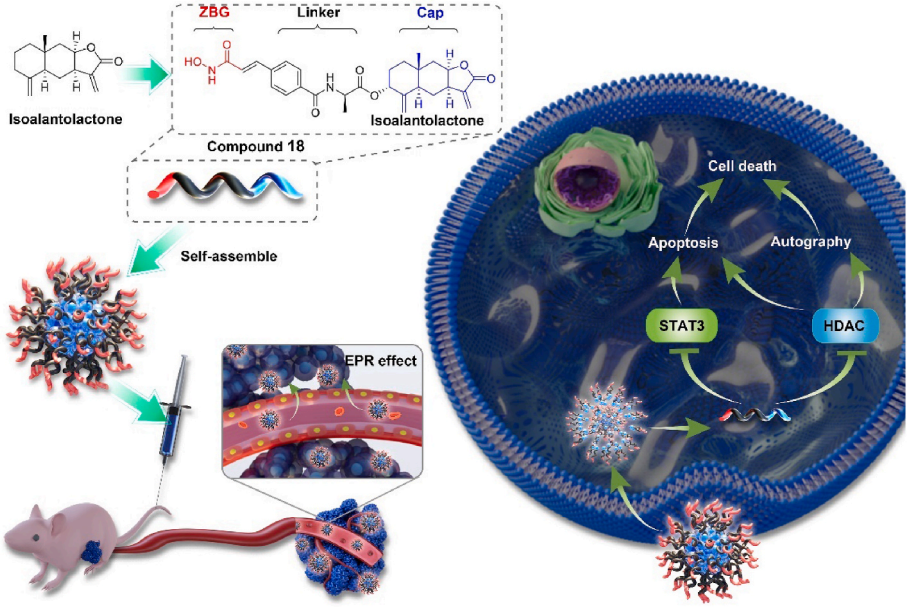

Scheme 1. Chemical structure of isoalantolactone/hydroxamic acid hybrids (compound **18**) and schematic representation for cellular uptake of hydroxamic acid hybrids nanoparticles and intracellular drug release. (i) Synthesis and self-assembly of supramolecular conjugate into nanoparticles in water. (ii) Nanoparticles enter cancer cells by endocytosis. (iii) Free hydroxamic acid hybrid was released in cells and (iv) targeted STAT3 and HDAC and induced autophagy and apoptosis.

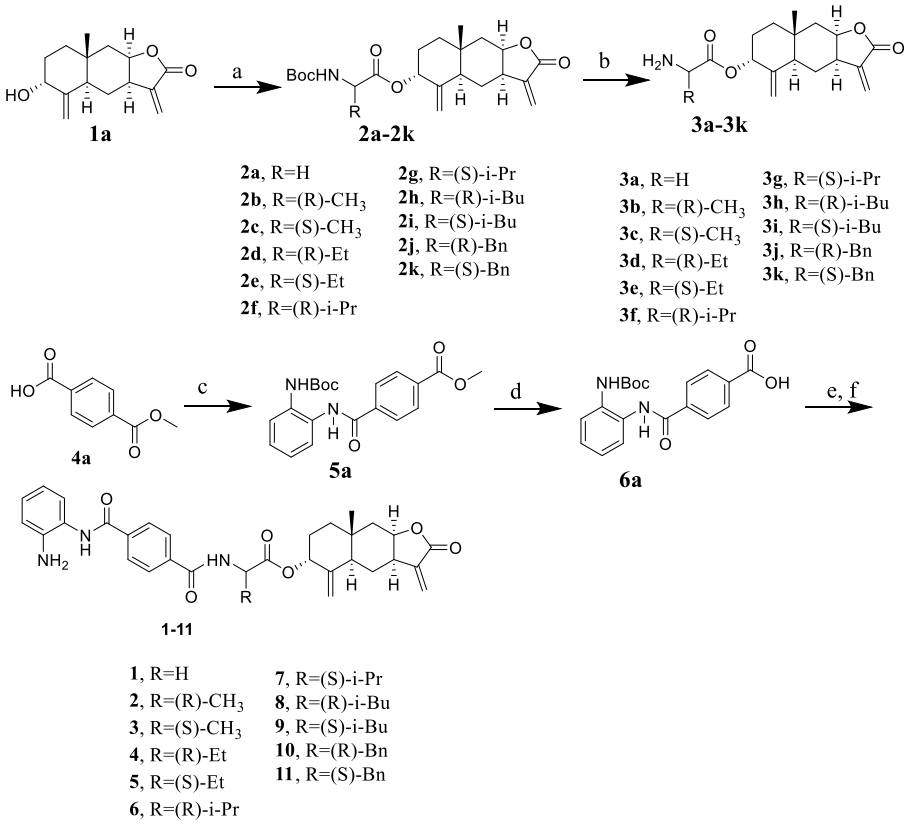

Scheme 2. Synthetic route of compounds **1**–**11**. Reagents and conditions (a) DIC, DMAP, CH_2Cl_2, rt, overnight,56%–88 %; (b) TFA, CH_2Cl_2, rt, 1 h, 85%–95 %; (c) HATU, DIPEA, DMF, rt, 8h, 63 %; (d) LiOH, H_2O, THF, RT, 8h, 90 %; (e) HATU, DIPEA, DMF, rt, 8 h; (f) TFA, CH_2Cl_2, rt, 1 h, 48%–65 % (e, f, two steps yield).

substitution also resulted in decreased activity. Interestingly, the 4-substituted N-hydroxycinnamamide **18** with (R)-CH_3 group exhibited superior HDACs inhibitor activity compared to that of compound **19** with (S)–CH_3 group and unsubstituted counterpart **15**. Among these hybrid compounds, N-hydroxycinnamamide **18**, characterized by an (R)-CH3 group, demonstrated outstanding activity against HDAC1, 2, 3, and 6. HDAC profiling revealed that compound **18** is a potent inhibitor against HDAC 8, 10, and 11. However, it fails to inhibit any class IIa HDACs (HDAC4, 5, 7, and 9) up to 10 μM (Table 2).

Additionally, surface plasmon resonance (SPR) binding assays were conducted to assess the binding capacity of compounds **1**–**19** with the recombinant STAT3 protein (Table 1). SPR analysis revealed that IAL directly bound to STAT3 with a equilibrium dissociation constant (K_D) value of 46.1 μM (Fig. S1, Supporting Information). In comparison to IAL, most of these hybrid compounds exhibited higher binding affinity, with K_D values at the low-micromolar level. Notably, **18** emerged as the most potent STAT3 inhibitor with a K_D value of 2.52 μM (Fig. 1A). In addition, **18** showed weak binding to STAT1, STAT2, STAT4, STAT5A, STAT5B, and STAT6 with K_D values of 19.2, 18.7, 42.5, 39.4, 23.3, 40.6, and 44.1 μM, respectively (Fig. S2, Supporting Information). Furthermoer, we also used a fluorescent polarization-based binding assay to evaluate the inhibitory activity of **18** against STAT3 [32]. As demonstrated in Figs. S3 and 18 could bind to STAT3 protein in a dose-dependent manner, with an IC_{50} value of 0.35 μM. This indicates that our design has successfully improved the activity towards both STAT3 and HDAC.

All synthesized hybrid compounds were evaluated for their cytotoxic activities against A549 cells (Table 3). N-hydroxycinnamamides **15**–**19** displayed heightened cytotoxic activities compared to compounds **1**–**14**. Among the N-hydroxycinnamamide derivatives, **18** demonstrated the highest activity against A549 cells (IC_{50} = 0.12 μM), which was more active than IAL and SAHA used alone or in combination (Table 2). The combination index (CI) was calculated using the Calcusyn software (Fig. S4, Supporting Information). The level of CI for A549 cells ranged from 0.405 to 0.600, demonstrating a synergistic effect of IAL and SAHA.

The antiproliferative properties of **18** were confirmed in HeLa, HCT116, and HepG2 cell lines. Overall, **18** exhibited superior antitumor activity compared to IAL and SAHA against three tumor cell lines (Table 4). Consequently, **18** was chosen for further experimentation.

2.2. Compound 18 targets STAT3 and HDAC in cancer cells

Western blot analysis suggested that **18** effectively suppressed the activation (phosphorylated form) of STAT3, while the same concentration of SAHA and IAL have little effect on the phosphorylation of STAT3 (Fig. 1B and C).

The cellular thermal shift assay (CETSA) showed that **18** directly interacted with STAT3 in A549 cells (Fig. 1D). Western blot analysis showed that 0.5 μM of **18** markedly increased Ac-tubulin and Ac-histone H3 levels suggesting that **18** inhibited class I HDACs and HDAC6 in the cellular environment (Fig. 2A and B). Molecular docking study revealed the binding mode of **18** with STAT3, HDAC1, and HDAC6 (Figs. S5–S7, Supporting Information). Together, these results demonstrated that **18** target STAT3 and HDAC.

Interestingly, when cells were treated with 4 μM of **18**, we observed that the level of Bcl-2 was not significantly changed (Fig. 1C), while the level of LC3-II was increased. Hence, we investigate the effect of **18** on autophagy and apoptosis.

2.3. 18 induces autophagy and apoptosis

Western blot analysis showed that 0.5 μM of **18** had little effect on the levels of Bcl-2 (Fig. 2A). When cells were treated with 0.5 μM of **18**,

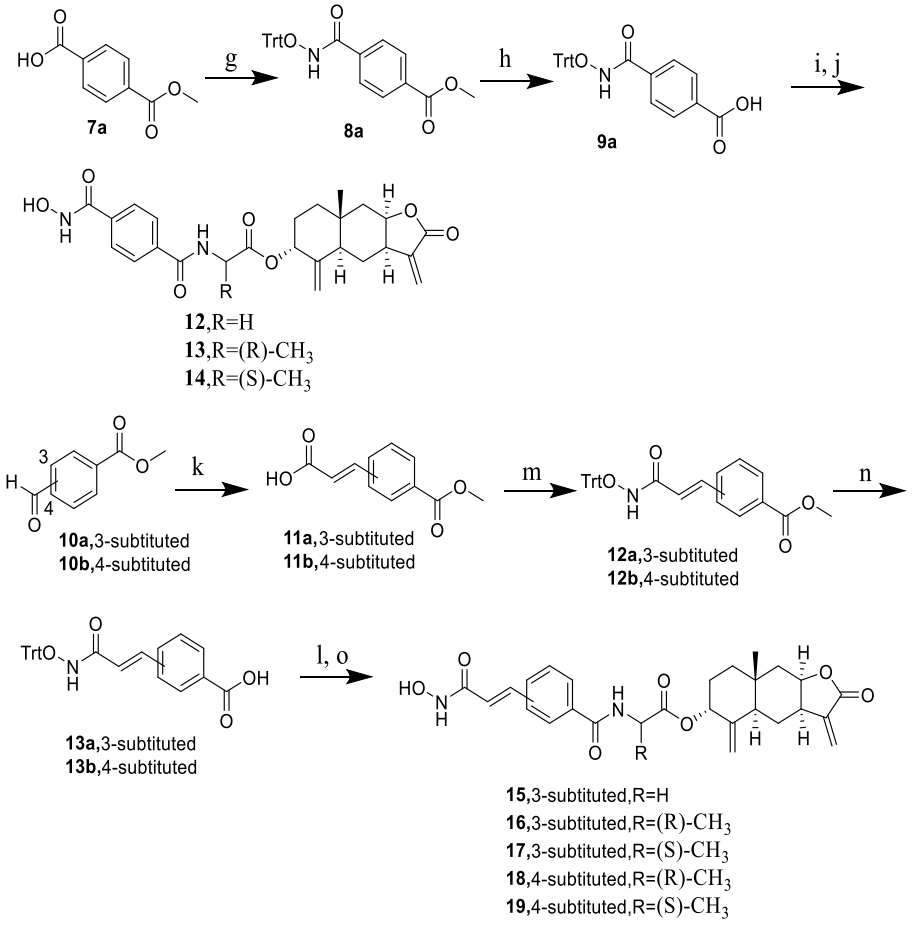

Scheme 3. Synthetic route of compounds **12**–**19**. Reagents and conditions: (g) HATU, DIPEA, DMF, rt, 8 h, 56 %; (h) LiOH, H_2O, THF, rt, 8 h, 91 %; (i) HATU, DIPEA, DMF, rt, 8h; (j) TFA, TES, rt, 15 min, 40%–54 % (i, j, two steps yield). (k) malonic acid, pyrimidine, DMF, 90 °C, 10 h, 90%–95 %; (m) HATU, DIPEA, DMF, rt, 8 h, 56–67 %; (n) LiOH, H_2O, THF, rt, 8 h, 88–93 %; (l) HATU, DIPEA, DMF, rt, 8 h; (o) TFA, TES, rt, 15min, 46%–45 % (l, o, two steps yield).

the P62 level decreased and the level of LC3-II was increased (Fig. 2C and D), and the LC3-II:LC3-I ratio increased in a time-dependent manner (Fig. 3A). Similar results were observed for the fluorescence signals of the tandem mRFP-GFP-LC3 (Fig. 4). The increased yellow (mRFP and GFP) and red puncta (mRFP only) indicating an intact autophagy flux induced by **18**.

Western blot analysis showed that only when the concentration of compound **18** was higher than 6 μM, the Bcl-2 level decreased significantly (Fig. 3B and C). The Annexin V-FITC/PI double-staining method was used to determine whether **18** also inhibited cancer cell proliferation by inducing apoptosis. The percentage of apoptotic cells in the **18** treatment groups reached 15 % (2 μM) and 40 % (4 μM, Fig. 5), respectively. These data suggest that low concentrations of **18** promoted autophagy-dependent cell death, whereas high concentrations promoted apoptosis.

2.4. Synthesis and characterization of 18 NPs

Due to its amphiphilic nature, **18** can self-assemble in water to form nanoparticles (**18** NPs). A stable white solution of **18** was obtained at a 1.0 mg/mL concentration. Dynamic light scattering (DLS) analysis showed that the average hydrodynamic diameters of compound **18** NPs were 85.6 ± 3.7 nm, and the surface charge of **18** NPs was −34.9 ± 2.5 mV (Fig. 6A). Transmission electron microscopy images showed that the average size of the nanoparticles was 68 nm, which was consistent with the DLS measurements (Fig. 6B). DLS measurements at different time intervals demonstrated that **18** NPs exhibited good stability in water and FBS solutions (Fig. 6C and D). Molecular dynamics simulation results indicated that hydrogen bonding may be the main driving force for forming **18** NPs (Fig. S8, Supporting Information).

2.5. Drug release behaviors of 18 NPs

The drug release behaviors of **18** NPs were evaluated in various buffer solutions. Fig. 6E shows that **18** NPs released less than 20 % within 24 h at pH 7.4, containing (or not) 10 % FBS, and 82 % at pH 5.0 after 24 h, indicating pH-dependent behavior. Meanwhile, **18** still remained steady at pH 5.0. This pH-responsive profile may benefit cancer therapy because of the weakly acidic tumor microenvironment.

2.6. Cellular uptake profiles of 18 NPs

To evaluate the cellular uptake ability of **18** NPs, chlorine e6 (Ce6)-loaded **18** NPs (**18**-Ce6 NPs), which can be used as probes for cell imaging, were prepared by the self-assembly of Ce6 and **18** (Fig. S9, Supporting Information). Confocal laser scanning microscopy showed that free Ce6 was hardly internalized by A549 cells (Fig. 7A). However, the red fluorescence of **18**-Ce6 NPs was stronger than that of free Ce6 after 4 h of treatment, suggesting that **18** NPs could improve the cellular uptake of drugs. The fluorescence intensity of the cells was quantitatively analyzed using flow cytometry (Fig. S10, Supporting Information). Fig. 7B shows that the cellular uptake of **18**-Ce6 NPs was significantly higher than that of free Ce6. These results demonstrated that **18** NPs could effectively penetrate through passive diffusion.

Table 1
Inhibitory activity of compounds **1**–**19** against HDAC1, HDAC2, HDAC3, and HDAC6, and the K_D values between compounds **1**–**19** and STAT3.

Compounds	IC_{50} (nM±SD)[a]				K_D (μM ±SD)
	HDAC1	HDAC2	HDAC3	HDAC6	STAT3
1	> 1000	> 1000	> 1000	> 1000	39.3 ± 5.14
2	122.3 ± 6.5	507.2 ± 46.0	472.9 ± 35.1	> 1000	4.96 ± 0.26
3	> 1000	> 1000	> 1000	> 1000	8.96 ± 0.79
4	6510.3 ± 35.2	> 1000	> 1000	> 1000	20.7 ± 1.59
5	> 1000	> 1000	> 1000	> 1000	22.6 ± 1.96
6	> 1000	> 1000	> 1000	> 1000	> 50
7	> 1000	> 1000	> 1000	> 1000	17.4 ± 2.01
8	452.7 ± 26.1	> 1000	> 1000	> 1000	6.88 ± 0.37
9	> 1000	> 1000	> 1000	> 1000	> 50
10	622.5 ± 39.2	> 1000	> 1000	> 1000	4.76 ± 0.27
11	> 1000	> 1000	> 1000	> 1000	> 50
12	201.7 ± 13.6	189.2 ± 15.9	107.1 ± 12.5	87.5 ± 6.3	> 50
13	748 ± 112	> 1000	> 1000	162.5 ± 18.5	20.1 ± 1.74
14	568.5 ± 49.3	843.8 ± 30.6	441.5 ± 42.7	267.4 ± 21.1	> 50
15	86.5 ± 7.9	92.7 ± 9.4	63.1 ± 8.8	45.3 ± 4.81	6.47 ± 0.93
16	197.4 ± 9.7	312.5 ± 25.0	102.6 ± 7.4	86.9 ± 1.1	13.5 ± 0.25
17	206.3 ± 12.5	404.2 ± 29.7	113.2 ± 8.1	62.4 ± 6.5	12.3 ± 0.25
18	62.0 ± 5.3	52.6 ± 4.3	51.9 ± 4.8	7.69 ± 0.69	2.52 ± 0.27
19	192.8 ± 13.5	341.7 ± 19.1	271.9 ± 24.6	64.0 ± 4.1	3.89 ± 0.52
SAHA	132.5 ± 11.7	120.4 ± 11.8	97.4 ± 8.6	24.5 ± 1.8	> 50
Chidamide	154.7 ± 23.8	212.5 ± 25.0	102.6 ± 7.4	> 1000	> 50
Isoalantolactone	> 1000	> 1000	> 1000	> 1000	46.1 ± 2.8

[a] Data are expressed as means ± SD (standard deviations) from at least three independent experiments.

2.7. In vitro anticancer efficacy of 18 NPs

The effects of **18** NPs on cell viability were evaluated in A549, HeLa, HCT116, and HepG2 cell lines. **18** NPs exhibited stronger inhibitory activity against these cancer cell lines than free **18**, with IC_{50} values ranged from 0.023 to 0.17 μM. Additionally, **18** NPs also caused apoptosis (Fig. 5) and autophagy (Fig. 4).

2.8. In vivo pharmacokinetics and biodistribution of 18 NPs

To confirm whether the **18** NPs had a longer blood retention time than **18**, we evaluated the pharmacokinetics of **18** and **18** NPs by monitoring the **18** concentration in blood. The concentration-time profiles in the blood showed that the **18** NPs had a higher concentration than IAL, free **18,** and the concentration of free **18** was only 1/10 of the **18** NPs after 12 h of administration (Fig. S11A, Supporting Information).

Subsequently, the A549 tumor-bearing nude mice were sacrificed to examine the amount of **18** NPs in the tumors and organs. The biodistribution profiles show that **18** NPs can more easily accumulate in tumor tissues, which supported that **18** NPs had better retention and accumulation properties than free **18** and IAL (Fig. S11B, Supporting Information).

Additionally, **18**-Ce6 NPs were used for *visualizing the biodistribution* of **18** NPs. Free Ce6 and **18**-Ce6 NPs were intravenously injected into A549 tumor-bearing nude mice. **18**-Ce6 NPs or free Ce6 can be rapidly distributed throughout the body upon intravenous injection. Compared to free Ce6, the **18**-Ce6 NPs maintained a high fluorescence intensity at the tumor sites, indicating the improved tumor-targeted accumulation and retention ability of **18** NPs (Fig. S11C, Supporting Information). Additionally, the *ex vivo* fluorescence images of tumors and organs at 24 h post-injection further supported that 18-Ce NPs had better retention and accumulation properties than free Ce6 (Fig. S11D, Supporting Information).

2.9. In vivo anticancer efficacy

In the pre-experiment, SAHA and **18** exhibited significant antitumor activities on A549 tumor-bearing nude mice, while IAL did not demonstrate significant antitumor activity (Fig. S12, Supporting Information). The antitumor efficacy of **18** NPs was further investigated. The tumor growth curves after administration of the control, 2.5, and 5 mg/kg of **18**, 10 mg/kg of SAHA, and 5 mg/kg of **18** NPs are shown in Fig. 8A. Compared with that of the control group, the tumor volume after 18 d of treatment was 70.7 ± 2.5 % for 2.5 mg/kg of **18**, 47.3 ± 3.4 % for 5 mg/kg of **18**, 61.0 ± 6.1 % for 10 mg/kg of SAHA, or 19.9 ± 2.1 % for **18** NPs, which suggested that **18** NPs had predominant tumor growth inhibitory efficacy than free **18** and SAHA. Western blot analysis was used to detect Ac-tubulin, Ac-histone H3, and phosphorylated STAT3 levels in the tumor tissue. These data demonstrated that **18** suppressed the phosphorylated of STAT3, inhibited and class I HDACs and HDAC6 (Fig. S13, Supporting information). Additionally, the lightest tumor weight was found in the **18** NPs treated group (Fig. 8B and C). Meanwhile, no apparent changes in body weight were observed in the different treatment groups, suggesting that **18** and **18** NPs did not lead to severe systemic toxicity (Fig. 8D). Furthermore, compared to the other groups, **18** NPs-treated tumors exhibited more necrosis, as shown by hematoxylin and eosin (H&E) staining, and more apoptosis, as shown by TUNEL staining (Fig. 9). H&E staining of the key organs in each group harvested at the end of the antitumor experiment revealed no obvious lesions (Fig. 10), further supporting the safety of **18** and **18** NPs.

3. Conclusions

In summary, herein, we reported a novel approach for modifying natural products. This led to the identification of **18**, a combination of isoalantolactone and hydroxamic acid, designed in the merged-molecule mode. Compound **18** showed excellent activity against both STAT3 and HDAC and exhibited better antitumor efficacy than isoalantolactone and hydroxamic acid SAHA, owing to the synergistic effect of STAT3 and

Table 2
HDAC isoform profiling of compound **18**.

Compounds	IC_{50} (nM ± SD)[a]						
	HDAC4	HDAC5	HDAC7	HDAC8	HDAC9	HDAC10	HDAC11
18	> 10000	> 10000	> 10000	1417 ± 74	> 10000	57.4 ± 8.1	265 ± 34
SAHA	> 10000	> 10000	> 10000	1530 ± 65	> 10000	81.3 ± 7.9	> 10000

[a] Data are expressed as means ± SD (standard deviations) from at least three independent experiments.

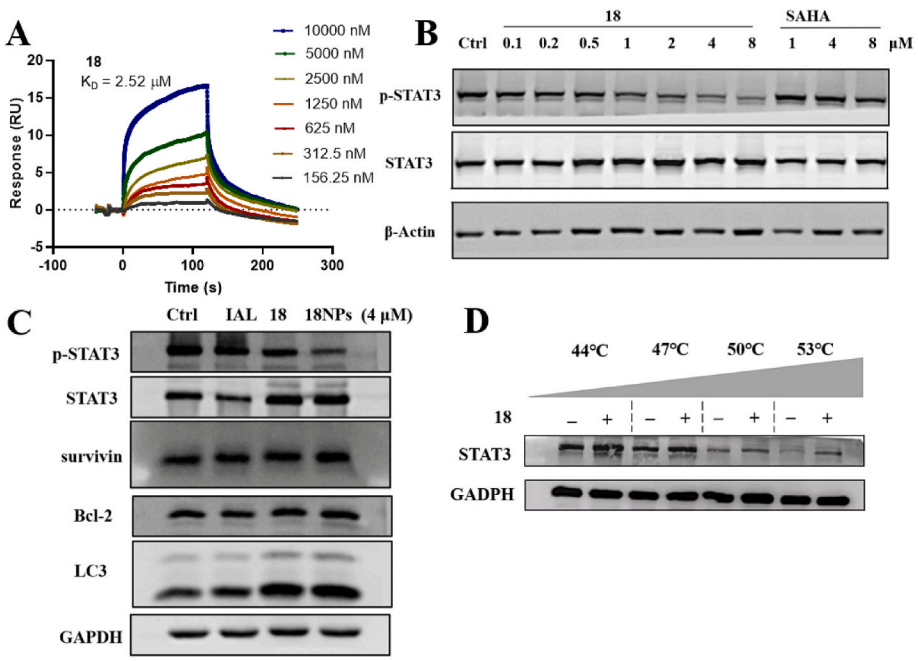

Fig. 1. Compound **18** target STAT3. (A) SPR analysis of **18** binding to STAT3 protein. (B) After treatment with **18** for 12 h, western blotting analysis of p-STAT3, STAT3 levels in A549 cells. (C) Western blotting analysis of p-STAT3, STAT3, survivin, and Bcl-2, levels in A549 cells treated with IAL, **18** and **18** NPs for 12 h. (D) The direct interactions of **18** with STAT3 in A549 cells were determined by CETSA (treatment with **18** at a concentration of 6 μM for 4 h).

Table 3
Antiproliferative activity[a] of target compounds **1**–**19** against A549 human cancer cell lines.

Compounds	IC_{50} (μM±SD)	Compounds	IC_{50} (μM±SD)
1	> 10	**13**	>10
2	2.24 ± 0.21	**14**	>10
3	3.34 ± 0.28	**15**	1.87 ± 0.09
4	6.67 ± 0.45	**16**	4.33 ± 0.31
5	> 10	**17**	4.53 ± 0.18
6	> 10	**18**	0.12 ± 0.02
7	> 10	**19**	4.53 ± 0.41
8	5.61 ± 0.43	**18** NPs	0.069 ± 0.002
9	> 10	IAL	1.81 ± 0.13
10	7.47 ± 0.53	chidamide	6.40 ± 0.54
11	> 10	SAHA	2.47 ± 0.32
12	2.56 ± 0.15	SAHA + IAL (1:1)	0.82 ± 0.08

[a] Data are expressed as means ± SD (standard deviations) from at least three independent experiments.

Table 4
Antiproliferative activity[a] of **18** and **18** NPs against different human cancer cell lines.

compound	Hela	HCT116	HepG2
IC_{50} (μM ± SD)[a]			
18	0.13 ± 0.01	0.040 ± 0.001	0.26 ± 0.01
18 NPs	0.072 ± 0.009	0.023 ± 0.002	0.17 ± 0.001
IAL	4.38 ± 0.08	2.61 ± 0.17	7.25 ± 0.16
SAHA	1.35 ± 0.13	1.87 ± 0.24	2.12 ± 0.17

[a] Data are expressed as means ± SD (standard deviations) from at least three independent experiments.

HDAC inhibitors. In addition, **18** self-assembled into nanoparticles in water. The **18** NPs exhibited better retention and accumulation properties than free **18**, resulting in superior anticancer efficacy. This demonstrates that the approach of combining the hydrophobic natural anticancer products isoalantolactone and hydroxamic acid not only has the advantage of being a dual-target drug but also has the advantage of self-assembled nanomedicine. Similar to conventional drugs, **18** has a smaller molecular weight than drug-drug conjugates. Furthermore, hydroxamic acid hybrids can synergize with various anticancer drugs. Overall, we believe that the strategy based on amphiphilic hydroxamic acid-based hybrids in the present study may open a new avenue for the rational design of dual-target drugs and the modification of natural products.

4. Experimental

4.1. Chemistry materials and methods

All commercial chemicals and solvents were of analytical grade and were used without further treatment unless otherwise noted. All reactions were carried out under an argon atmosphere. ^{1}H NMR and ^{13}C NMR spectra were recorded with a Bruker AVANCE III 500 MHz spectrometer. The HRMS data were recorded with a Q Exactive Orbitrap-MS apparatus (Thermo, USA). Silica gel (200–300mesh, Qingdao Marine Chemical Factory, Qingdao, PR China). Purity of the final compounds were determined using an ACQUITY Arc system (Waters Co, USA) with a C-18 column (Sunfire, 5 μm, 4.6 mm × 250 mm) and were found to be ≥ 95 %, unless otherwise stated.

4.2. Chemical synthesis and structural characterization of the target compounds

4.2.1. (3aR,4aR,6R,8aR,9aR)-8a-methyl-3,5-dimethylene-2-oxododecahydronaphtho[2,3-b]furan-6-yl (tert-butoxycarbonyl)glycinate (2a)

Compound **1a** (248 mg, 1 mmol) was dissolved in CH_2Cl_2 (5 mL). DMAP (12.2 mg, 0.1 mmol), DIC (154 mg, 1.2 mmol) and BOC-glycine (175 mg, 1 mmol) were added to this solution. After stirred at room temperature overnight, the reaction mixture was filtered. The filtrate was then washed with saturated $NaHCO_3$ solution, dried over anhydrous Na_2SO_4, and evaporated under reduced pressure. The crude product was purified by column chromatography to obtain compound **2a** (White solid, 227 mg, 56 % yield). ^{1}H NMR (500 MHz, Chloroform-*d*) δ 6.15 (s,

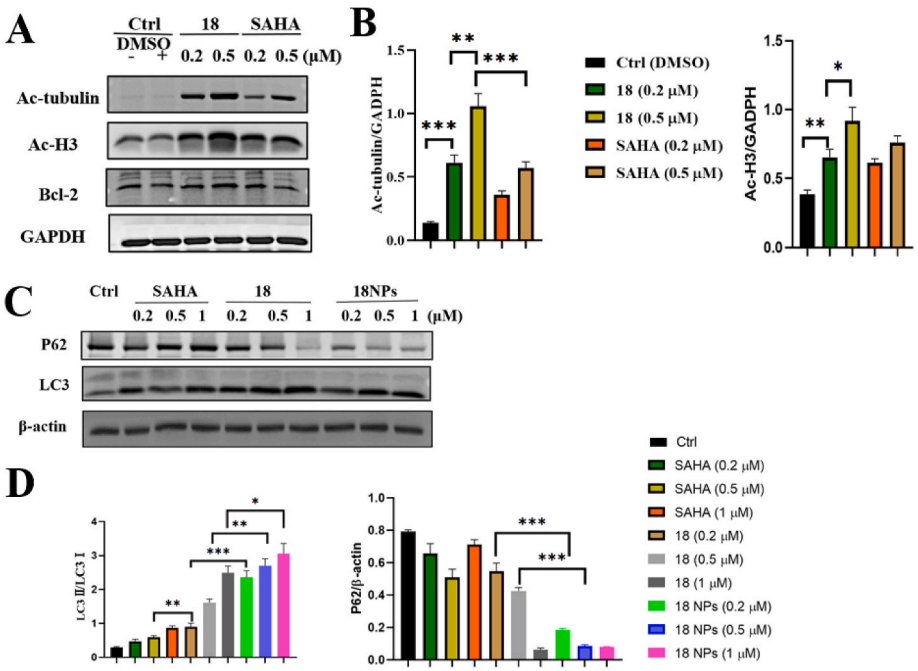

Fig. 2. (A) Western blotting analysis of Bcl-2 levels in A549 cells treated with the indicated concentration of **18** for 12 h. (B) Quantitative analysis of ac-tubulin and ac-histone H3 levels, normalized against GAPDH. *P < 0.05, **P < 0.01, and ***P < 0.001. (B) Western blotting analysis of LC3 and P62 levels in A549 cells treated with the **18**, **18** NPs, and SAHA for 12 h. SAHA was used as a positive control. (D) Quantitative analysis of Fig. 2C. *P < 0.05, **P < 0.01, and ***P < 0.001.

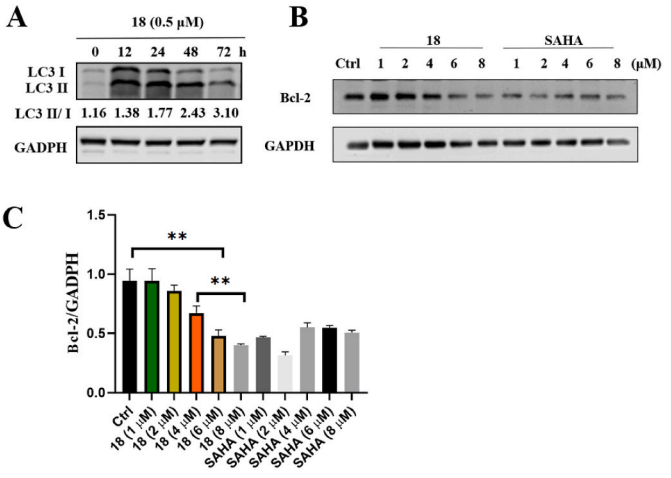

Fig. 3. (A) The LC3-II:LC3-I ratio of A549 cells at the indicated time after treatment with **18** (0.5 μM). (B) Western blotting analysis of Bcl-2 levels in A549 cells treated with the indicated concentration of **18** for 12 h. (C) Quantitative analysis of Fig. 3B. *P < 0.05, **P < 0.01, and ***P < 0.001.

1H), 5.60 (s, 1H), 5.42 (s, 1H), 5.15 (s, 1H), 4.73 (s, 1H), 4.54–4.50 (m, 1H), 3.90 (d, J = 5.5 Hz, 2H), 3.06–2.98 (m, 1H), 2.25–2.16 (m, 2H), 1.86–1.79 (m, 2H), 1.72 (ddd, J = 14.0, 7.1, 2.6 Hz, 1H), 1.60–1.51 (m, 4H), 1.45 (s, 9H), 1.43–1.32 (m, 2H), 0.84 (s, 3H).

2b-2k were synthesized in the same way as **2a**.

4.2.2. (3aR,4aR,6R,8aR,9aR)-8a-methyl-3,5-dimethylene-2-oxododecahydronaphtho[2,3-b]furan-6-yl (tert-butoxycarbonyl)-R-alaninate (2b)

Compound **2b** (White solid, 270 mg, 78 % yield) was prepared following the same synthetic procedure of compound **2a**.^{1}H NMR (500 MHz, Chloroform-*d*) δ 6.15 (s, 1H), 5.61 (s, 1H), 5.38 (s, 1H), 5.15 (s, 1H), 5.04 (d, J = 8.1 Hz, 1H), 4.73 (s, 1H), 4.56–4.50 (m, 1H), 4.30 (t, J = 7.4 Hz, 1H), 3.06–2.98 (m, 1H), 2.27–2.20 (m, 2H), 2.18 (d, J = 2.5 Hz, 1H), 1.89–1.76 (m, 2H), 1.72 (ddd, J = 13.9, 7.1, 2.6 Hz, 1H), 1.59–1.55 (m, 2H), 1.44 (s, 9H), 1.36 (d, J = 7.2 Hz, 3H), 1.34–1.24 (m, 2H), 0.84 (s, 3H).

4.2.3. (3aR,4aR,6R,8aR,9aR)-8a-methyl-3,5-dimethylene-2-oxododecahydronaphtho[2,3-b]furan-6-yl (tert-butoxycarbonyl)-S-alaninate (2c)

Compound **2c** (White solid, 240 mg, 82 % yield) was prepared following the same synthetic procedure of compound **2a.**^{1}H NMR (500 MHz, Chloroform-*d*) δ 6.15 (s, 1H), 5.61 (s, 1H), 5.38 (s, 1H), 5.15 (s, 1H), 5.10 (d, J = 7.9 Hz, 1H), 4.73 (s, 1H), 4.54–4.51 (m, 1H), 4.34–4.28 (m, 1H), 3.07–2.99 (m, 1H), 2.23 (d, J = 15.4 Hz, 2H), 1.84–1.79 (m , 2H), 1.74–1.70 (m, 1H), 1.55 (d, J = 4.8 Hz, 2H), 1.44 (s, 9H), 1.40 (d, J = 7.2 Hz, 3H), 1.38–1.31 (m, 2H), 0.84 (s, 3H).

4.2.4. (3aR,4aR,6R,8aR,9aR)-8a-methyl-3,5-dimethylene-2-oxododecahydronaphtho[2,3-b]furan-6-yl (R)-2-((tert-butoxycarbonyl) amino)butanoate (2d)

Compound **2d**(White solid, 140 mg, 72 % yield) was prepared following the same synthetic procedure of compound **2a**. ^{1}H NMR (500 MHz, Chloroform-*d*) δ 6.15 (s, 1H), 5.60 (s, 1H), 5.40 (s, 1H), 5.14 (s, 1H), 5.05 (d, J = 7.9 Hz, 1H), 4.72 (s, 1H), 4.55–4.49 (m, 1H), 4.25 (q, J = 7.1 Hz, 1H), 3.04–2.96 (m, 1H), 2.26–2.15 (m, 2H), 1.87–1.78 (m, 3H), 1.74–1.64 (m, 3H), 1.59–1.55 (m, 1H), 1.44 (s, 9H), 1.40–1.32 (m, 2H), 0.89 (t, J = 7.6 Hz, 3H), 0.83 (s, 3H).

4.2.5. (3aR,4aR,6R,8aR,9aR)-8a-methyl-3,5-dimethylene-2-oxododecahydronaphtho[2,3-b]furan-6-yl (S)-2-((tert-butoxycarbonyl) amino)butanoate (2e)

Compound **2e**(White solid, 156 mg, 70 % yield) was prepared following the same synthetic procedure of compound **2a.**^{1}H NMR (500 MHz, Chloroform-*d*) δ 6.15 (s, 1H), 5.61 (s, 1H), 5.40 (s, 1H), 5.15 (s, 1H), 5.09 (d, J = 8.4 Hz, 1H), 4.73 (s, 1H), 4.55–4.50 (m, 1H), 4.30–4.22 (m, 1H), 3.08–3.00 (m, 1H), 2.27–2.19 (m, 2H), 1.89–1.79 (m, 3H), 1.76–1.65 (m, 3H), 1.60–1.50 (m, 3H), 1.44 (s, 9H), 1.42–1.31 (m, 3H), 0.94 (t, J = 7.4 Hz, 3H), 0.84 (s, 3H).

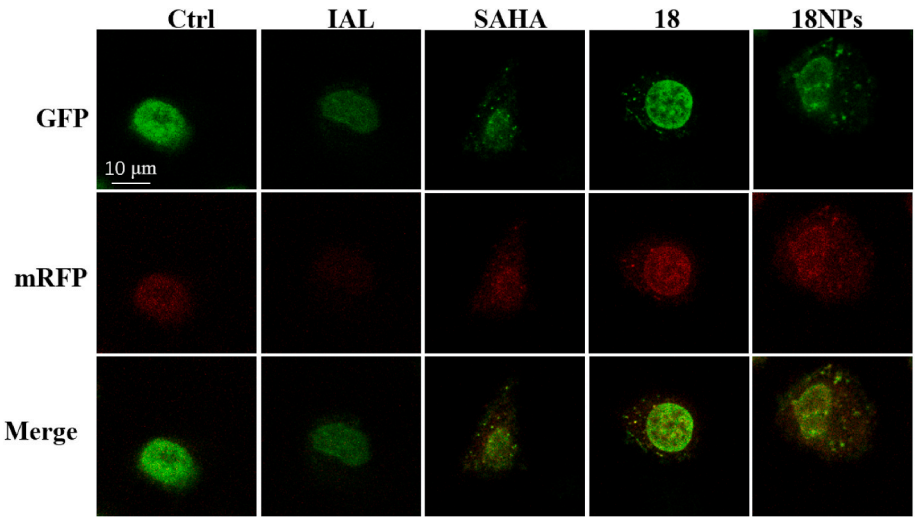

Fig. 4. **18** induced intact autophagy flux. A549 cells were transfected with tandem mRFP-GFP-LC3B plasmid, then incubated with 0.5 μM of SAHA, IAL, **18**, and **18** NPs for 24 h, followed by confocal microscope photography.

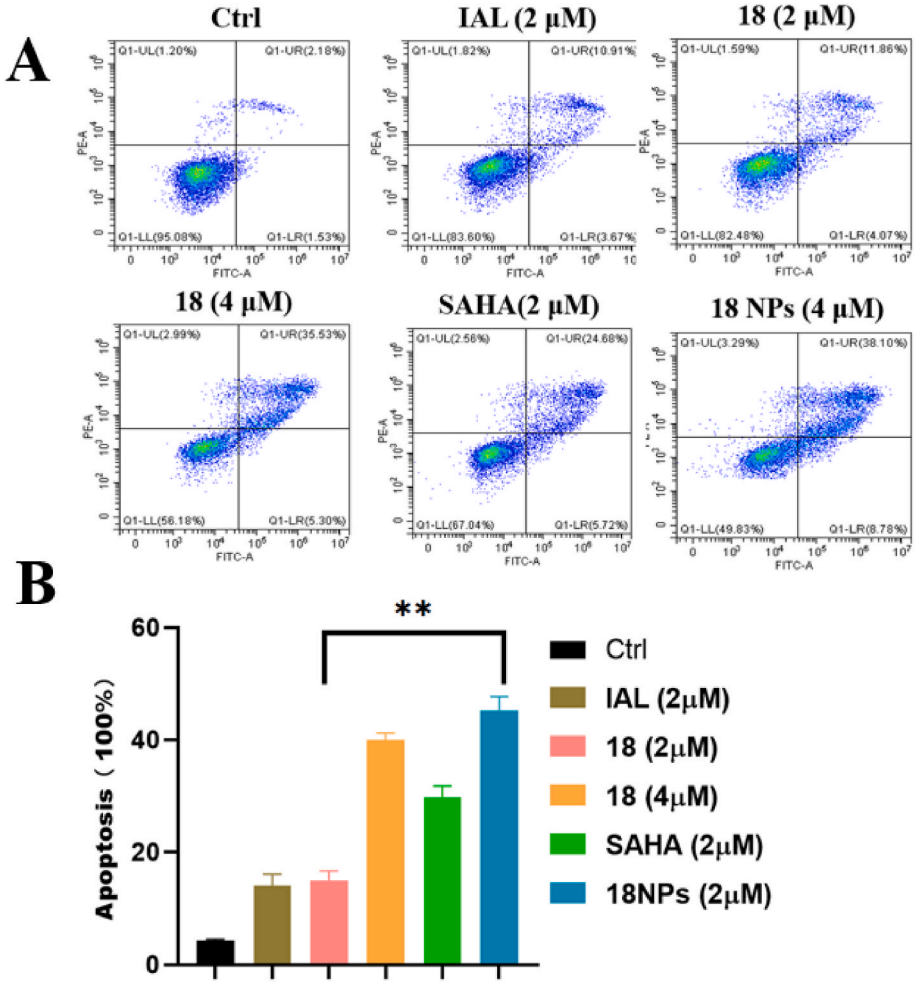

Fig. 5. Cell apoptosis induced by compound **18.** (A) After incubation with **18** and **18** NPs for 24 h, A549 cells were analyzed using flow cytometry. (B) Quantitative analysis of Fig. 5A. **P < 0.01.

4.2.6. (3aR,4aR,6R,8aR,9aR)-8a-methyl-3,5-dimethylene-2-oxododecahydronaphtho[2,3-b]furan-6-yl (tert-butoxycarbonyl)-R-valinate (2f)

Compound **2f** (White solid, 278 mg, 88 % yield) was prepared following the same synthetic procedure of compound **2a**.[1]H NMR (500 MHz, Chloroform-*d*) δ 6.15 (s, 1H), 5.61 (s, 1H), 5.41 (s, 1H), 5.15 (s, 1H), 5.03 (d, J = 9.2 Hz, 1H), 4.72 (s, 1H), 4.56–4.50 (m, 1H), 4.21 (dd, J = 9.1, 4.7 Hz, 1H), 3.04–2.95 (m, 1H), 2.27–2.18 (m, 2H), 2.15–2.06

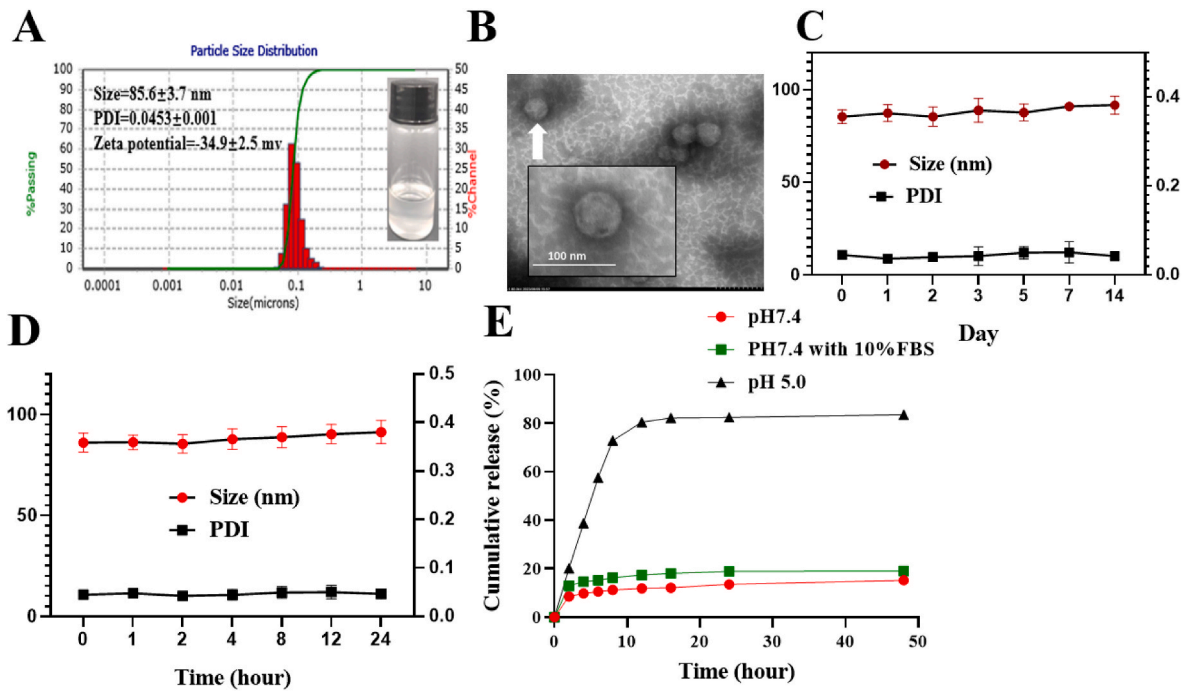

Fig. 6. Characterization of **18** NPs. (A) DLS for **18** NPs. (B) The TEM photograph of **18** NPs. (C) Measurements of diameter and PDI of **18** NPs in PBS during storage at 4 °C for 14 days. (D) Measurements of diameter and PDI of 18 NPs in PBS containing 10 % FBS at 37 °C for 24 h. Samples were measured in triplicates. (E) *In vitro* release kinetics from **18** NPs at different pH values (5.0 and 7.4) containing 10 % FBS (or not) at 37 °C.

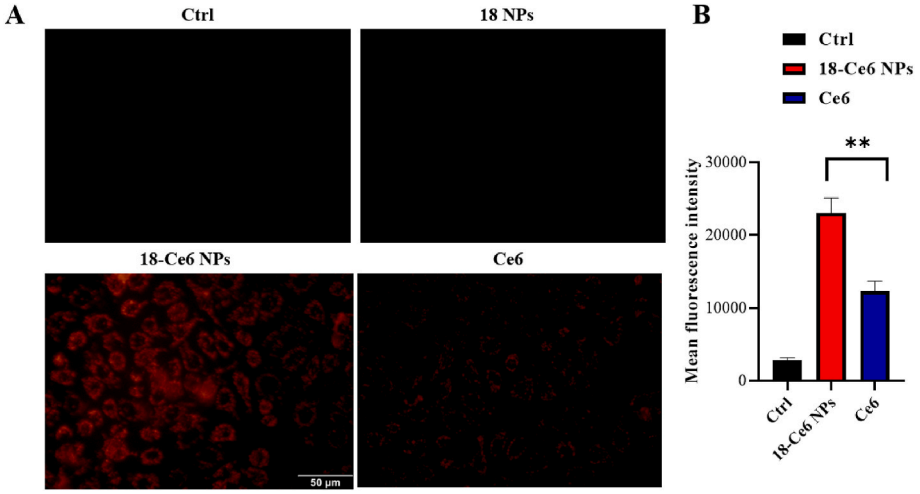

Fig. 7. Cellular uptake profiles of **18** NPs in A549 cells. (A) Fluorescence images of A549 cells incubated with **18**-Ce6 NPs, **18** NPs, and Ce6 for 4 h. (B) Mean fluorescence intensity in the A549 cells by flow cytometry analysis.

(m, 1H), 1.87–1.78 (m, 2H), 1.69 (ddd, J = 14.0, 7.1, 2.8 Hz, 1H), 1.44 (s, 9H),1.42–1.30 (m, 2H), 0.95 (d, J = 6.9 Hz, 6H), 0.84 (s, 3H).

4.2.7. (3aR,4aR,6R,8aR,9aR)-8a-methyl-3,5-dimethylene-2-oxododecahydronaphtho[2,3-b]furan-6-yl (tert-butoxycarbonyl)-S-valinate (2g)

Compound **2g (**White solid, 228 mg, 85 % yield**)** was prepared following the same synthetic procedure of compound **2a**. ^{1}H NMR (500 MHz, Chloroform-*d*) δ 6.15 (s, 1H), 5.61 (s, 1H), 5.41 (s, 1H), 5.15 (s, 1H), 5.08 (d, J = 9.1 Hz, 1H), 4.73 (s, 1H), 4.56–4.50 (m, 1H), 4.22 (dd, J = 9.1, 4.5 Hz, 1H), 3.09–3.01 (m, 1H), 2.28–2.20 (m, 2H), 2.18–2.09 (m, 1H), 1.87–1.70 (m, 4H), 1.57–1.52 (m, 1H), 1.44 (s, 9H),1.40–1.30 (m, 2H), 0.97 (d, J = 6.9 Hz, 3H), 0.89 (d, J = 6.9 Hz, 3H), 0.84 (s, 3H).

4.2.8. (3aR,4aR,6R,8aR,9aR)-8a-methyl-3,5-dimethylene-2-oxododecahydronaphtho[2,3-b]furan-6-yl (tert-butoxycarbonyl)-R-leucinate (2h)

Compound **2h(**White solid, 375 mg, 81 % yield**)** was prepared following the same synthetic procedure of compound **2a**.^{1}H NMR (500 MHz, Chloroform-*d*) δ 6.15 (s, 1H), 5.61 (s, 1H), 5.38 (s, 1H), 5.14 (s, 1H), 4.90 (d, J = 8.9 Hz, 1H), 4.72 (s, 1H), 4.53 (t, J = 4.6 Hz, 1H), 4.33–4.27 (m, 1H), 3.02–2.96 (m, 1H), 2.26–2.17 (m, 2H), 1.90–1.79 (m, 2H), 1.74–1.65 (m, H), 1.52–1.48 (m, 1H), 1.44 (s, 8H), 1.41–1.34 (m, 2H), 0.94 (d, J = 6.6 Hz, 6H), 0.84 (s, 3H).

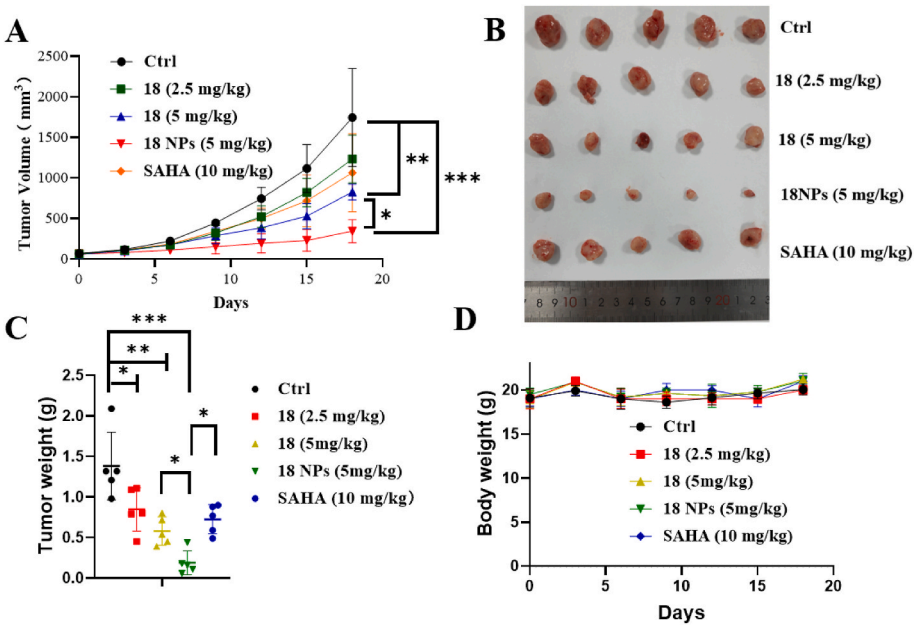

Fig. 8. *In vivo* antitumor activity of **18** in the A549 xenograft model. (A) Growth curve of implanted A549 xenograft in nude mice. (B) Tumor photographs separated from mice after different treatments. (C) Mean weight of tumors dissected in the end of treatments. (E) The body weight changes of the mice after treatment with PBS, **18** (2.5 mg/kg), **18** (5 mg/kg), **18** NPs (5 mg/kg), and SAHA (10 mg/kg).

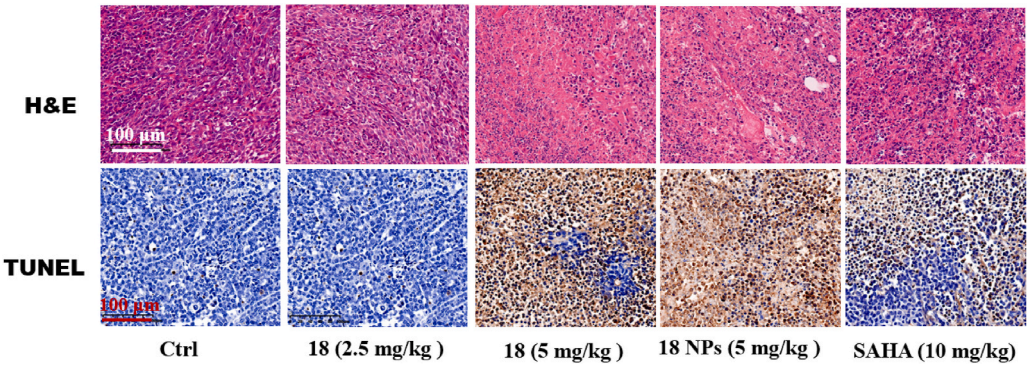

Fig. 9. H&E stain and TUNEL stain of analysis of tumor tissues after treated with PBS, SAHA, **18**, and **18** NPs.

4.2.9. (3aR,4aR,6R,8aR,9aR)-8a-methyl-3,5-dimethylene-2-oxododecahydronaphtho[2,3-b]furan-6-yl (tert-butoxycarbonyl)-S-leucinate (2i)

Compound **2i** (White solid, 183 mg, 83 % yield)was prepared following the same synthetic procedure of compound **2a**.^{1}H NMR (500 MHz, Chloroform-*d*) δ 6.15 (s, 1H), 5.61 (s, 1H), 5.38 (s, 1H), 5.15 (s, 1H), 4.96 (d, J = 8.9 Hz, 1H), 4.73 (s, 1H), 4.55–4.52 (m, 1H), 4.34–4.28 (m, 1H), 3.07–3.01 (m, 1H), 2.27–2.20 (m, 2H), 1.84–1.79 (m, 2H), 1.75–1.67 (m, 2H), 1.58–1.55 (m, 1H), 1.44 (s, 9H), 1.36–1.25 (m, 2H), 0.96 (d, J = 6.6 Hz, 6H), 0.84 (s, 3H).

4.2.10. (3aR,4aR,6R,8aR,9aR)-8a-methyl-3,5-dimethylene-2-oxododecahydronaphtho[2,3-b]furan-6-yl (tert-butoxycarbonyl)-R-phenylalaninate (2j)

Compound **2j** (White solid, 203 mg, 79 % yield) was prepared following the same synthetic procedure of compound **2a**.^{1}H NMR (500 MHz, Chloroform-*d*) δ 7.30–7.21 (m, 3H), 7.10 (d, J = 7.1 Hz, 2H), 6.14 (s, 1H), 5.60 (s, 1H), 5.38 (s, 1H), 5.13 (s, 1H), 5.02 (d, J = 8.3 Hz, 1H), 4.72 (s, 1H), 4.61–4.53 (m, 1H), 4.52–4.46 (m, 1H), 3.10–2.92 (m, 3H), 2.18 (d, J = 15.1 Hz, 1H), 1.97 (d, J = 12.4 Hz, 1H), 1.65 (ddd, J = 14.0, 7.1, 2.7 Hz, 1H), 1.48 (dd, J = 15.5, 4.8 Hz, 2H), 1.42 (s, 9H), 1.38–1.17 (m, 4H), 0.80 (s, 3H).

4.2.11. (3aR,4aR,6R,8aR,9aR)-8a-methyl-3,5-dimethylene-2-oxododecahydronaphtho[2,3-b]furan-6-yl (tert-butoxycarbonyl)-L-phenylalaninate (2k)

Compound **2k** was prepared following the general synthetic procedure of compound **2a**(White solid, 326 mg, 84 % yield).

4.2.12. General procedure for the synthesis of compounds 3a-3k

The intermediate 2a-2k (1 mmol) were dissolved in CH_2Cl_2 (4 mL), and trifluoroacetic acid (2 mL) was added to the reaction. The reaction mixture was stirred for 1h at room temperature. Then, the reaction mixture was evaporated under the reduced pressure to provide a yellow solid **3a-3k** (Yield, 85%–95 %), which were used in the following step without further purification.

4.2.13. Methyl 4-((2-((tert-butoxycarbonyl)amino)phenyl)carbamoyl) benzoate (5a)

mono-Methyl terephthalate (**4a**, 554 mg, 3.08 mmol) was dissolved in 10 mL DMF, HATU (1.4 g, 3.7 mmol), *tert*-Butyl (2-Aminophenyl) carbamate (640 mg, 3.08 mmol), and DPIEA (1.5 mL, 9.24 mmol) were added. This mixture was stirred under nitrogen protection for 8 h, poured into water, and extracted with ethyl acetate. Organics were combined and washed with 5 % citric acid, saturated $NaHCO_3$ solution

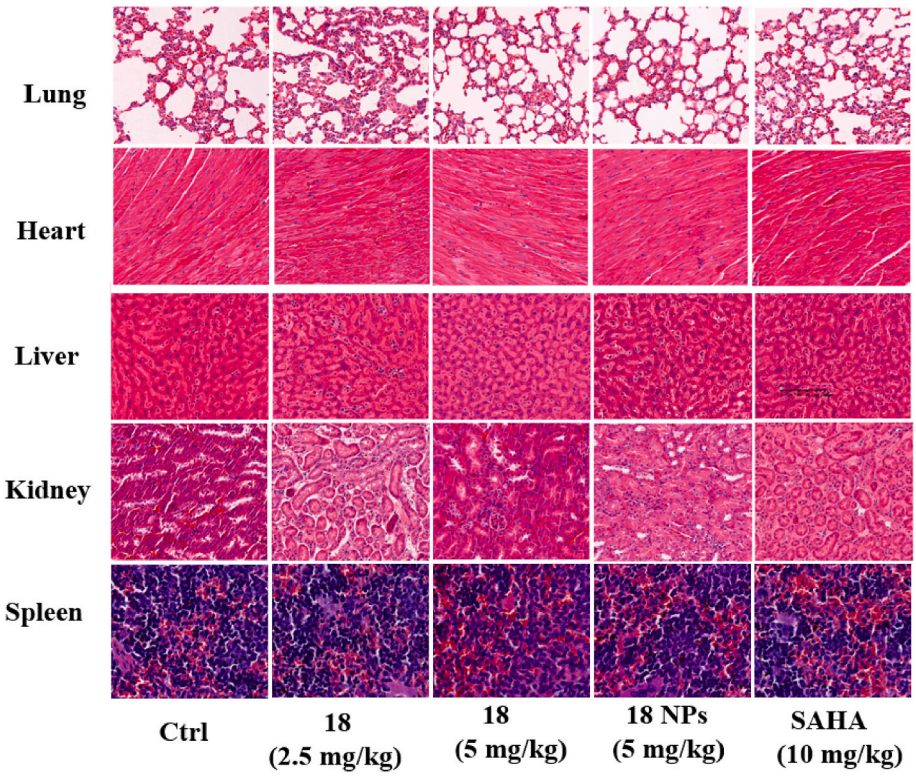

Fig. 10. H&E staining of heart, liver, spleen, and lung of the mice after treatment with PBS, **18** (2.5 mg/kg), **18** (5 mg/kg), **18** NPs (5 mg/kg), and SAHA (10 mg/kg).

and brine, dried over anhydrous $MgSO_4$, filtered, and evaporated to provide the crude product. The crude product was purified by column chromatography to obtain compound **5a** (White solid, 718 mg, 63 %).^{1}H NMR (500 MHz, Chloroform-*d*) δ 9.44 (s, 1H), 8.16–8.10 (d, J = 8.2 Hz, 2H), 8.03 (d, J = 8.2 Hz, 2H), 7.87 (d, J = 8.0 Hz, 1H), 7.21–7.13 (m, 2H), 6.72 (s, 1H), 3.96 (s, 3H), 1.52 (s, 9H).

4.2.14. 4-((2-((tert-butoxycarbonyl) amino)phenyl)carbamoyl)benzoic acid (6a)

5a (500 mg, 1.40 mmol) and lithium hydroxide (134 mg, 5.6 mmol) were dissolved in a mixture of water (8 mL) and THF (2 mL). After stirring for 8 h, THF in this solution was evaporated. The mixture was adjusted to pH 7 and extracted with ethyl acetate. After drying over anhydrous $MgSO_4$, it was filtered and evaporated to obtain ompound **6a** (White solid, 467 mg, 90 %).^{1}H NMR (500 MHz, DMSO-d_6) δ 13.30 (s, 1H), 9.97 (s, 1H), 8.73 (s, 1H), 8.11–8.02 (m, 4H), 7.55 (ddd, J = 13.7, 7.9, 1.6 Hz, 2H), 7.21 (td, J = 7.7, 1.6 Hz, 1H), 7.15 (td, J = 7.6, 1.6 Hz, 1H), 1.44 (s, 9H).

4.2.15. (3aR,4aR,6R,8aR,9aR)-8a-methyl-3,5-dimethylene-2-oxododecahydronaphtho[2,3-b]furan-6-yl (4-((2-aminophenyl)carbamoyl) benzoyl)glycinate (1)

6a (356 mg, 1 mmol) was dissolved in 10 mL DMF, HATU (456 mg, 1.2 mmol), **3a** (305 mg, 1 mmol), and DPIEA (0.52 mL, 3 mmol) were added. This mixture was stirred under nitrogen protection for 8 h, poured into water, and extracted with ethyl acetate. Organics were combined and washed with 5 % citric acid, saturated $NaHCO_3$ solution and brine, dried over anhydrous $MgSO_4$, filtered, and evaporated to provide the crude product. The crude product was purified by column chromatography to obtain intermediate. The intermediate (0.5 mmol) were dissolved in CH_2Cl_2 (2 mL), and trifluoroacetic acid (1 mL) was added to the reaction. The reaction mixture was stirred for 1h at room temperature. The mixture was adjusted to pH 8 and extracted with ethyl acetate. After drying over anhydrous $MgSO_4$, it was filtered and evaporated to obtain compound **1** (yellow solid, 258 mg, 48 %).^{1}H NMR (500 MHz, Chloroform-*d*) δ 8.30 (m, 1H), 7.93–7.76 (m, 4H), 7.31 (d, J = 7.0 Hz, 1H), 7.09 (t, J = 7.5 Hz, 1H), 7.05–6.97 (m, 1H), 6.83 (d, J = 7.0 Hz, 2H), 6.13 (s, 1H), 5.60 (s, 1H), 5.44 (d, J = 3.2 Hz, 1H), 5.16 (s, 1H), 4.75 (s, 1H), 4.50 (s, 1H), 4.18 (d, J = 5.5 Hz, 2H), 3.03–2.94 (m, 1H), 2.21 (d, J = 14.2 Hz, 2H), 1.89–1.77 (m , 2H), 1.74–1.67 (m, 1H), 1.64–1.50 (m, 2H), 1.45–1.21 (m, 4H), 0.83 (s, 3H). ^{13}C NMR (125 MHz, $CDCl_3$) δ 170.64,169.23, 166.75, 165.09, 145.00, 141.90, 140.84, 137.19, 136.55, 127.82, 127.57, 125.45, 124.40, 120.73, 119.91, 118.58, 113.51, 76.67, 42.24, 41.52, 40.96, 40.40, 36.33, 33.97, 27.11, 26.97, 17.15. HRMS(ESI) *m/z* calced for $C_{31}H_{34}N_3O_6$ [M+H] + 544.2442, found 544.2435.

4.2.16. (3aR,4aR,6R,8aR,9aR)-8a-methyl-3,5-dimethylene-2-oxododecahydronaphtho[2,3-b]furan-6-yl (4-((2-aminophenyl)carbamoyl) benzoyl)-R-alaninate (2)

Compound **2** (yellow solid, 243 mg, 51 %) was prepared following the same synthetic procedure of compound **1**.^{1}H NMR (500 MHz, Chloroform-*d*) δ 8.39 (s, 1H), 7.87 (d, J = 7.9 Hz, 2H), 7.79 (d, J = 8.0 Hz, 2H), 7.30 (d, J = 7.9 Hz, 1H), 6.85–6.75 (m, 1H), 7.04 (d, J = 7.2 Hz, 1H), 6.82 (d, J = 7.8 Hz, 2H), 6.13 (s, 1H), 5.60 (s, 1H), 5.40 (s, 1H), 5.16 (s, 1H), 4.78–4.69 (m, 2H), 4.52–4.46 (m, 1H), 3.93 (s, 2H), 3.03–2.95 (m , 1H), 2.24–2.15 (m, 2H), 1.89–1.79 (m, 2H), 1.71 (ddd, J = 14.0, 7.1, 2.7 Hz, 1H), 1.61–1.50 (m, 2H), 1.47 (d, J = 7.3 Hz, 3H), 1.44–1.21 (m, 5H), 0.82 (s, 3H).^{13}C NMR (126 MHz, $CDCl_3$) δ 172.27, 170.62, 166.21, 165.13, 145.01, 141.90, 140.92, 137.14, 136.70, 127.80, 127.55, 127.50, 125.50, 124.40, 120.70, 119.81, 118.53, 113.40, 76.65, 48.95, 41.60, 40.97, 40.41, 36.37, 33.94, 27.02, 27.00, 18.37, 17.09. HRMS(ESI) *m/z* calced for $C_{32}H_{36}N_3O_6$ $[M+H]^+$558.2598 , found 558.2591.

4.2.17. (3aR,4aR,6R,8aR,9aR)-8a-methyl-3,5-dimethylene-2-oxododecahydronaphtho[2,3-b]furan-6-yl (4-((2-aminophenyl)carbamoyl) benzoyl)-S-alaninate (3)

Compound **3** (yellow solid, 57 mg, 54 %) was prepared following the same synthetic procedure of compound **1** .^{1}H NMR (500 MHz,

Chloroform-*d*) δ 8.37 (s, 1H), 7.87 (d, *J* = 7.9 Hz, 2H), 7.78 (d, *J* = 8.0 Hz, 2H) , 7.31 (d, *J* = 7.8 Hz, 1H), 7.11–6.99 (m, 2H), 6.87–6.76 (m, 2H), 6.12 (s, 1H), 5.58 (s, 1H), 5.41 (s, 1H), 5.16 (s, 1H), 4.81–4.68 (m, 2H), 4.53–4.44 (m, 1H), 3.92 (s, 2H), 3.00–2.90 (m, 1H), 2.26–2.17 (m, 2H), 1.87–1.80 (m, 2H), 1.69 (ddd, *J* = 14.0, 7.1, 2.7 Hz, 1H), 1.60–1.47 (m, 5H), 1.45–1.40 (m, 1H), 1.36–1.29 (m, 1H), 0.83 (s, 3H).^{13}C NMR (125 MHz, $CDCl_3$) δ 172.32, 170.64, 166.10, 165.09, 144.93, 141.87, 140.91, 137.16, 136.70, 127.78, 127.51, 125.46, 124.43, 120.75, 119.80, 118.52, 113.48,77.06, 76.65, 48.86, 41.53, 41.00, 40.33, 36.41, 33.95, 27.14, 26.93, 18.71, 17.12. HRMS(ESI) *m/z* calced for $C_{32}H_{36}N_3O_6$ $[M+H]^+$558.2598 , found 558.2590.

4.2.18. (3aR,4aR,6R,8aR,9aR)-8a-methyl-3,5-dimethylene-2-oxododecahydronaphtho[2,3-b] furan-6-yl (R)-2-(4-((2-aminophenyl) carbamoyl) benzamido)butanoate (4)

Compound **4** (yellow solid, 38 mg, 49 %) was prepared following the same synthetic procedure of compound **1** .^{1}H NMR (500 MHz, Chloroform-*d*) δ 8.42 (s, 1H), 7.88 (d, *J* = 8.0 Hz, 2H), 7.79 (d, *J* = 8.0 Hz, 2H), 7.30 (d, *J* = 7.8 Hz, 1H), 7.08 (t, *J* = 7.6 Hz, 1H), 6.98 (d, *J* = 7.6 Hz, 1H), 6.84–6.77 (m, 2H), 6.13 (s, 1H), 5.60 (s, 1H), 5.43 (s, 1H), 5.16 (s, 1H), 4.78–4.69 (m, 2H), 4.49 (td, *J* = 4.8, 1.7 Hz, 1H), 3.88 (s, 2H), 3.02–2.93 (m, 1H), 2.19 (t, *J* = 14.0 Hz, 2H), 2.02–1.92 (m, 1H), 1.89–1.77 (m, 3H), 1.69 (ddd, *J* = 14.0, 7.1, 2.7 Hz, 1H), 1.62–1.48 (m, 2H), 1.45–1.36 (m, 1H), 1.36–1.30 (m, 1H), 0.93 (t, *J* = 7.4 Hz, 3H), 0.82 (s, 3H).^{13}C NMR (125 MHz, $CDCl_3$) δ 171.70, 170.61, 166.45, 165.14, 145.05, 141.89, 140.93, 137.15, 136.79, 127.82, 127.49, 125.51, 124.41, 120.71, 119.77, 118.49, 113.42, 77.00, 76.64, 54.05, 41.69, 40.96, 40.41, 36.40, 33.92, 27.01, 26.98, 25.72, 17.07, 9.59. HRMS(ESI) *m/z* calced for $C_{33}H_{38}N_3O_6$ $[M+H]^+$572.2755 , found 572.2755.

4.2.19. (3aR,4aR,6R,8aR,9aR)-8a-methyl-3,5-dimethylene-2-oxododecahydronaphtho[2,3-b]furan-6-yl(S)-2-(4-((2-aminophenyl) carbamoyl)benzamido)butanoate (5)

Compound **5** (yellow solid, 62 mg, 57 %) was prepared following the same synthetic procedure of compound **1** .^{1}H NMR (500 MHz, Chloroform-*d*) δ 8.41 (s, 1H), 7.88 (d, *J* = 8.0 Hz, 2H), 7.79 (d, *J* = 8.0 Hz, 2H), 7.31 (d, *J* = 7.8 Hz, 1H), 7.08 (td, *J* = 7.7, 1.5 Hz, 1H), 7.00 (d, *J* = 7.8 Hz, 1H), 6.85–6.78 (m, 2H), 6.11 (s, 1H), 5.58 (s, 1H), 5.43 (s, 1H), 5.15 (s, 1H), 4.79–4.71 (m, 2H), 4.52–4.46 (m, 1H), 4.21–3.47 (m, 2H), 3.02–2.93 (m, 1H), 2.26–2.17 (m, 2H), 2.06–1.97 (m, 1H), 1.89–1.78 (m, 3H), 1.69 (ddd, *J* = 14.0, 7.1, 2.7 Hz, 1H), 1.60–1.51 (m, 2H), 1.47–1.39 (m,1H), 1.35–1.29 (m, 1H), 0.99 (t, *J* = 7.4 Hz, 3H), 0.83 (s, 3H).^{13}C NMR (125 MHz, $CDCl_3$) δ 171.74, 170.67, 166.39, 165.13, 144.95, 141.86, 140.90, 137.17, 136.76, 127.80, 127.50, 125.48, 124.42, 120.76, 119.78, 118.50, 113.47, 77.01, 76.67, 53.97, 41.52, 41.00, 40.31, 36.45, 33.95, 27.24, 26.92, 25.96, 17.13, 9.73. HRMS (ESI) *m/z* calced for $C_{33}H_{38}N_3O_6$ $[M+H]^+$572.2755 , found 572.2751.

4.2.20. (3aR,4aR,6R,8aR,9aR)-8a-methyl-3,5-dimethylene-2-oxododecahydronaphtho[2,3-b]furan-6-yl (4-((2-aminophenyl)carbamoyl) benzoyl)-R-valinate (6)

Compound **6** (yellow solid, 83 mg, 60 %)was prepared following the same synthetic procedure of compound **1** .^{1}H NMR (500 MHz, Chloroform-*d*) δ 8.28 (s, 1H), 7.93 (d, *J* = 7.7 Hz, 2H), 7.83 (d, *J* = 8.0 Hz, 2H), 7.33 (d, *J* = 8.0 Hz, 1H), 7.09 (t, *J* = 7.4 Hz, 1H), 6.88–6.78 (m, 3H), 6.14 (s, 1H), 5.62 (s, 1H), 5.45 (s, 1H), 5.17 (s, 1H), 4.80–4.68 (m, 2H), 4.53–4.48 (m, 1H), 3.91 (s, 2H), 3.02–2.95 (m, 1H), 2.29–2.17 (m, 3H), 1.87–1.82 (m, 2H), 1.69 (ddd, *J* = 14.0, 7.0, 2.7 Hz, 1H), 1.62–1.52 (m, 2H), 1.46–1.41 (m, 1H), 1.37–1.32 (m, 1H), 1.28–1.22 (m, 1H), 0.98 (dd, *J* = 22.6, 6.8 Hz, 6H), 0.83 (s, 3H). ^{13}C NMR (125 MHz, $CDCl_3$) δ 171.35, 170.61, 166.66, 165.04, 145.06, 141.90, 140.81, 137.22, 137.03, 127.85, 127.55, 125.40, 124.47, 120.72, 119.91, 118.60, 113.50, 76.95, 76.64, 57.70, 41.82, 40.99, 40.46, 36.45, 33.93, 31.96, 27.03, 26.98, 19.10, 17.97, 17.10. HRMS(ESI) *m/z* calced for $C_{34}H_{40}N_3O_6$ $[M+H]^+$586.2912 , found 586.2903.

4.2.21. (3aR,4aR,6R,8aR,9aR)-8a-methyl-3,5-dimethylene-2-oxododecahydronaphtho[2,3-b]furan-6-yl (4-((2-aminophenyl)carbamoyl) benzoyl)-S-valinate (7)

Compound **7** (yellow solid, 49 mg, 62 %) was prepared following the same synthetic procedure of compound **1** .^{1}H NMR (500 MHz, Chloroform-*d*) δ 8.44 (s, 1H), 7.88 (d, *J* = 8.0 Hz, 2H), 7.77 (d, *J* = 8.0 Hz, 2H), 7.31 (d, *J* = 7.8 Hz, 1H), 7.10–7.04 (m, 1H), 6.91 (d, *J* = 8.6 Hz, 1H), 6.84–6.77 (m, 2H), 6.11 (s, 1H), 5.58 (s, 1H), 5.45 (s, 1H), 5.15 (s, 1H), 4.80–4.70 (m, 2H), 4.51–4.47 (m, 1H), 3.92 (s, 2H), 3.02–2.96 (m, 1H), 2.31–2.19 (m, 3H), 1.91–1.77 (m, 2H), 1.69 (ddd, *J* = 14.0, 7.0, 2.7 Hz, 1H), 1.59–1.51 (m, 2H), 1.48–1.40 (m, 1H), 1.34–1.29 (m, 1H), 1.01 (dd, *J* = 11.1, 6.8 Hz, 6H), 0.82 (s, 3H).^{13}C NMR (125 MHz, $CDCl_3$) δ 171.32, 170.68, 166.66, 165.15, 144.94, 141.86, 140.91, 137.19, 136.84, 127.81, 127.47, 125.49, 124.40, 120.76, 119.72, 118.44, 113.47, 76.96, 76.68, 57.68, 41.51, 40.99, 40.28, 36.49, 33.93, 31.94, 27.28, 26.90, 19.13, 18.03, 17.14. HRMS(ESI) *m/z* calced for $C_{34}H_{40}N_3O_6$ $[M+H]^+$586.2912 , found 586.2902.

4.2.22. (3aR,4aR,6R,8aR,9aR)-8a-methyl-3,5-dimethylene-2-oxododecahydronaphtho[2,3-b]furan-6-yl (4-((2-aminophenyl)carbamoyl) benzoyl)-R-leucinate (8)

Compound **8** (yellow solid, 45 mg, 58 %) was prepared following the same synthetic procedure of compound **1** .^{1}H NMR (500 MHz, Chloroform-*d*) δ 8.61 (s, 1H), 7.94–7.68 (m, 4H), 7.33–7.24 (m, 1H), 7.14–7.00 (m, 2H), 6.87–6.73 (m, 2H), 6.13 (s, 1H), 5.61 (s, 1H), 5.41 (s, 1H), 5.15 (s, 1H), 4.82–4.70 (m, 2H), 4.55–4.43 (m, 1H), 3.94 (s, 2H), 3.00–2.92 (m, 1H), 2.23–2.14 (m, 2H), 1.89–1.80 (m, 2H), 1.74–1.59 (m, 4H), 1.53–1.44 (m, 1H), 1.43–1.24 (m, 3H), 0.96 (dd, *J* = 6.1, 2.1 Hz, 6H), 0.82 (s, 3H).^{13}C NMR (125 MHz, $CDCl_3$) δ 172.41, 170.64, 166.60, 165.20, 145.05, 141.87, 141.02, 137.00, 136.62, 127.77, 127.52, 127.46, 125.63, 124.37, 120.70, 119.70, 118.45, 113.29, 76.99, 76.66, 51.77, 41.63, 41.17, 40.93, 40.40, 36.37, 33.87, 27.00, 26.96, 25.14, 22.88, 22.31, 17.05. HRMS(ESI) *m/z* calced for $C_{35}H_{42}N_3O_6$ $[M+H]^+$600.3068 , found 600.3064.

4.2.23. (3aR,4aR,6R,8aR,9aR)-8a-methyl-3,5-dimethylene-2-oxododecahydronaphtho[2,3-b]furan-6-yl (4-((2-aminophenyl)carbamoyl) benzoyl)-S-leucinate(9)

Compound **9** (yellow solid, 56 mg, 63 %) was prepared following the same synthetic procedure of compound **1** .^{1}H NMR (500 MHz, Chloroform-*d*) δ 8.56 (s, 1H), 7.82 (d, *J* = 8.0 Hz, 2H), 7.73 (d, *J* = 7.9 Hz, 2H), 7.28 (d, *J* = 7.6 Hz, 1H), 7.10–7.01 (m, 2H), 6.80 (d, *J* = 8.4 Hz, 2H), 6.10 (s, 1H), 5.58 (s, 1H), 5.40 (s, 1H), 5.14 (s, 1H), 4.85–4.77 (m, 1H), 4.72 (s, 1H), 4.47 (t, *J* = 4.8 Hz, 1H), 3.93 (s, 2H), 3.00–2.91 (m, 1H), 2.20 (t, *J* = 14.3 Hz, 2H), 1.85–1.77 (m, 2H), 1.73–1.64 (m, 3H), 1.58–1.46 (m, 2H), 1.45–1.37 (m, 1H), 1.33–1.23 (m, 2H), 0.98 (d, *J* = 6.2 Hz, 6H), 0.81 (s, 3H).^{13}C NMR (125 MHz, $CDCl_3$) δ 172.55, 170.72, 166.41, 165.10, 144.93, 141.82, 140.95, 137.00, 136.56, 127.73, 127.46, 125.53, 124.39, 120.80, 119.74, 118.48, 113.45, 76.69, 51.53, 41.68, 41.45, 40.97, 40.22, 36.44, 33.91, 27.19, 26.89, 25.19, 22.90, 22.24, 17.12. HRMS(ESI) *m/z* calced for $C_{35}H_{42}N_3O_6$ $[M+H]^+$600.3068 , found 600.3060.

4.2.24. (3aR,4aR,6R,8aR,9aR)-8a-methyl-3,5-dimethylene-2-oxododecahydronaphtho[2,3-b]furan-6-yl(4-((2-aminophenyl)carbamoyl) benzoyl)-R-phenylalaninate (10)

Compound **10** (yellow solid, 68 mg, 65 %) was prepared following the same synthetic procedure of compound **1** .^{1}H NMR (500 MHz, Chloroform-*d*) δ 8.05 (s, 1H), 7.94 (d, *J* = 8.0 Hz, 2H), 7.79 (d, *J* = 8.0 Hz, 2H), 7.36 (d, *J* = 7.8 Hz, 1H), 7.29–7.26 (m, 3H), 7.14–7.08 (m, 3H), 6.90–6.82 (m, 2H), 6.72 (d, *J* = 7.6 Hz, 1H), 6.16 (s, 1H), 5.62 (s, 1H), 5.46 (s, 1H), 5.19 (s, 1H), 5.08 (q, *J* = 5.9 Hz, 1H), 4.79 (s, 1H), 4.50 (t, *J* = 4.1 Hz, 1H), 3.28–3.19 (m, 2H), 3.00–2.94 (m, 1H), 2.21 (d , *J* = 15.6 Hz, 1H), 2.06 (d , *J* = 13.0 Hz , 1H), 1.86–1.79 (m, 2H), 1.70 (ddd, *J* = 13.9, 7.1, 2.7 Hz, 1H), 1.53–1.45 (m, 2H), 1.42–1.37 (m, 1H), 1.33 (t, *J* = 6.1 Hz, 1H), 0.83 (s, 3H).^{13}C NMR (125 MHz, $CDCl_3$) δ 170.75,

170.58, 166.00, 164.92, 145.07, 141.97, 140.65, 137.29, 136.88, 135.82, 129.54, 128.73, 127.84, 127.57, 127.35, 125.27, 124.54, 120.67, 120.12, 118.76, 113.52, 77.24, 76.62, 53.73, 41.70, 40.97, 40.41, 38.13, 36.37, 33.92, 27.10, 27.06, 17.14. HRMS(ESI) *m/z* calced for $C_{38}H_{40}N_3O_6$ $[M+H]^+$634.2912 , found 634.2904.

4.2.25. (3aR,4aR,6R,8aR,9aR)-8a-methyl-3,5-dimethylene-2-oxododecahydronaphtho[2,3-b]furan-6-yl(4-((2-aminophenyl)carbamoyl) benzoyl)-S-phenylalaninate (11)

Compound **11** (yellow solid, 51 mg, 63 %) was prepared following the same synthetic procedure of compound **1**. ^{1}H NMR (500 MHz, Chloroform-*d*) δ 8.23 (d, J = 7.8 Hz, 1H), 7.89 (d, J = 7.7 Hz, 2H), 7.75 (d, J = 7.9 Hz, 2H), 7.35–7.23 (m, 5H), 7.17 (d, J = 7.0 Hz, 1H), 7.13–7.06 (m , 1H), 6.84 (d, J = 6.0 Hz, 2H), 6.13 (s, 1H), 5.59 (s, 1H), 5.40 (s, 1H), 5.13 (s, 1H), 5.10–5.03 (m, 1H), 4.72 (s, 1H), 4. 51–4.45 (m, 1H), 3.90 (s, 2H), 3.29–3.17 (m, 2H), 3.01–2.92 (m, 1H), 2.17–2.10 (m, 3H), 1.84–1.74 (m, 2H), 1.73–1.64 (m, 3H), 1.47 (dd, J = 15.6, 4.9 Hz, 1H), 1.40–1.20 (m, 6H), 0.81 (s, 3H).^{13}C NMR (125 MHz, $CDCl_3$) δ 170.93, 170.64, 166.05, 164.98, 144.88, 141.89, 140.78, 137.24, 136.73, 135.90, 129.42, 128.81, 127.81, 127.57, 127.51, 127.41, 125.36, 124.45, 120.73, 119.95, 118.63, 113.52, 76.65, 53.86, 41.43, 40.94, 40.34, 38.52, 36.34, 33.90, 27.16, 26.90, 17.14. HRMS(ESI) *m/z* calced for $C_{38}H_{40}N_3O_6$ $[M+H]^+$634.2912, found 634.2902.

4.2.26. Methyl 4-((trityloxy)carbamoyl)benzoate (8a)

Compound **8a** (yellow solid, 203 mg, 56 % yield) **w**as prepared following the same synthetic procedure of compound **5a** .^{1}H NMR (500 MHz, DMSO-d_6) δ 13.17 (s, 1H), 11.13 (s, 1H), 7.41 (d, J = 7.4Hz, 2H), 7.37–7.27 (m, 17H).

4.2.27. 4-((trityloxy)carbamoyl)benzoic acid (9a)

Compound **9a w**as prepared following the general synthetic procedure of compound 6**a**.^{1}H NMR (500 MHz, DMSO-d_6) δ 13.17 (s, 1H), 11.13 (s, 1H), 7.41 (d, J = 7.4Hz, 2H), 7.37–7.27 (m, 17H).

4.2.28. (3aR,4aR,6R,8aR,9aR)-8a-methyl-3,5-dimethylene-2-oxododecahydronaphtho[2,3-b]furan-6-yl (4-(hydroxycarbamoyl)benzoyl) glycinate (12)

9a (423 mg, 1 mmol) was dissolved in 10 mL DMF, HATU (456 mg, 1.2 mmol), **3a** (305 mg, 1 mmol), and DPIEA (0.52 mL, 3 mmol) were added. This mixture was stirred under nitrogen protection for 8 h, poured into water, and extracted with ethyl acetate. Organics were combined and washed with 5 % citric acid, saturated $NaHCO_3$ solution and brine, dried over anhydrous $MgSO_4$, filtered, and evaporated to provide the crude product. The crude product was purified by column chromatography to obtain intermediate. The intermediate (0.5 mmol) were dissolved in CH_2Cl_2 (5 mL), trifluoroacetic acid (0.1 mL) and triethylsilane (0.1 mL) was added to the reaction. The reaction mixture was stirred for 15min at room temperature. Then, add 50 mL of the mixed solution of n-hexane: Petroleum ether: ether (10:10:1), and collect by filtration to obtain compound **12**(yellow solid, 187 mg, 40 %).^{1}H NMR (500 MHz, DMSO-d_6) δ 11.36 (s, 1H), 9.17 (s, 1H), 9.10 (t, J = 6.0 Hz, 1H), 7.96 (d, J = 8.1 Hz, 2H), 7.86 (d, J = 8.1 Hz, 2H), 5.97 (s, 1H), 5.74 (s, 1H), 5.29 (s, 1H), 5.09 (s, 1H), 4.68 (s, 1H), 4.42 (td, J = 4.9, 1.6 Hz, 1H), 4.02 (d, J = 5.9 Hz, 2H), 2.90 (dt, J = 12.0, 6.1 Hz, 1H), 2.16–2.10 (m, 1H), 1.99–1.92 (m, 1H), 1.78–1.64 (m, 2H), 1.59 (ddd, J = 13.9, 7.2, 2.5 Hz, 1H), 1.51–1.41 (m , 1H), 1.31–1.23 (m, 2H), 1.11 (q, J = 12.8 Hz, 1H), 0.69 (s, 3H).^{13}C NMR (125 MHz, DMSO) δ 169.91, 168.62, 166.06, 163.42, 145.53, 142.06, 135.87, 135.50, 127.42, 127.06, 120.48, 112.26, 76.18, 75.49, 41.82, 40.53, 35.48, 33.39, 26.61, 26.37, 16.79. HRMS(ESI) *m/z* calced for $C_{25}H_{29}N_2O_7$ $[M+H]^+$469.1969, found 469.1972.

4.2.29. (3aR,4aR,6R,8aR,9aR)-8a-methyl-3,5-dimethylene-2-oxododecahydronaphtho[2,3-b]furan-6-yl (4-(hydroxycarbamoyl) benzoyl)-R-alaninate (13)

Compound **13** (yellow solid, 25 mg, 51 %) was prepared following the same synthetic procedure of compound **12** .^{1}H NMR (500 MHz, DMSO-d_6) δ 11.36 (s, 1H), 8.91 (d, J = 7.1 Hz, 1H), 7.98 (d, J = 8.5 Hz, 2H), 7.85 (d, J = 8.4 Hz, 2H), 5.96 (s, 1H), 5.76 (s, 1H), 5.25 (s, 1H), 5.07 (s, 1H), 4.66 (s, 1H), 4.51–4.43 (m,1H), 4.42–4.37 (m, 1H), 2.91–2.83 (m, 1H), 2.08 (d, J = 12.8 Hz, 1H), 1.93 (d, J = 14.6 Hz, 1H), 1.78–1.64 (m, 2H), 1.61–1.53(ddd, J = 13.9, 7.2, 2.6 Hz, 1H), 1.51–1.42 (m, 1H), 1.41 (d, J = 7.3 Hz, 3H), 1.31–1.24 (m, 1H), 1.20 (dd, J = 15.6, 4.8 Hz, 1H), 1.14–1.04 (m, 1H), 0.68 (s, 3H).^{13}C NMR (126 MHz, DMSO) δ 171.33, 169.90, 165.71, 163.37, 145.55, 142.03, 135.93, 135.38, 127.57, 126.90, 120.50, 112.10, 76.14, 75.28, 48.81, 40.47, 35.56, 33.36, 26.60, 26.34, 16.74, 16.50. HRMS(ESI) *m/z* calced for $C_{26}H_{31}N_2O_7$ $[M+H]^+$483.2126, found 483.2128.

4.2.30. (3aR,4aR,6R,8aR,9aR)-8a-methyl-3,5-dimethylene-2-oxododecahydronaphtho[2,3-b]furan-6-yl (4-(hydroxycarbamoyl) benzoyl)-R-alaninate (14)

Compound **14** (yellow solid, 56 mg, 54 %) was prepared following the same synthetic procedure of compound **12** .^{1}H NMR (500 MHz, DMSO-d_6) δ 11.36 (s, 1H), 9.17 (s, 1H), 8.91 (d, J = 7.3 Hz, 1H), 7.98 (d, J = 8.2 Hz, 2H), 7.86 (d, J = 8.1 Hz, 2H), 5.96 (s, 1H), 5.71 (s, 1H), 5.24 (s, 1H), 5.10 (s, 1H), 4.67 (s, 1H), 4.51 (p, J = 7.3 Hz, 1H), 4.38 (td, J = 4.9, 1.7 Hz, 1H), 2.77 (dt, J = 12.0, 6.4 Hz, 1H), 2.11 (dd, J = 12.6, 2.4 Hz, 1H), 1.93 (dd, J = 15.7, 1.7 Hz, 1H), 1.76–1.69 (m, 1H), 1.65 (dt, J = 14.4, 3.6 Hz, 1H), 1.57 (ddd, J = 13.9, 7.1, 2.6 Hz, 1H), 1.45–1.35 (m, 4H), 1.29–1.18 (m, 2H), 1.10 (q, J = 12.8 Hz, 1H), 0.67 (s, 3H).^{13}C NMR (126 MHz, DMSO) δ 171.32, 169.91, 165.74, 163.43, 145.56, 142.03, 135.99, 135.45, 127.63, 126.96, 120.47, 112.12, 76.17, 75.54, 48.69, 40.59, 35.43, 33.38, 26.55, 26.37, 16.78, 16.53. HRMS(ESI) *m/z* calced for $C_{26}H_{31}N_2O_7$ $[M+H]^+$483.2126, found 483.2128.

4.2.31. (E)-3-(3-(Methoxycarbonyl)phenyl)acrylic acid (11a)

A mixture of methyl 4-formylbenzoate (0.82 g, 5 mmol), malonic acid (1.56 g, 15 mmol), pyrimidine (0.4 mL), and DMF (20 mL) was heated to 90 °C under nitrogen protection and stirred for 10 h. The solution was quenched by 60 mL water and kept in an ice bath to precipitate the product. **11a**(white solid, 979 mg, 95 %) was obtained by filtration. ^{1}H NMR (500 MHz, Chloroform-*d*) δ 8.24 (s, 1H), 8.08 (d, J = 7.7 Hz, 1H), 7.90–7.68 (m, 2H), 7.58–7.47 (m, 1H), 6.54 (d, J = 16.4 Hz, 1H), 3.95 (s, 3H).

4.2.32. (E)-3-(4-(Methoxycarbonyl)phenyl)acrylic acid (11b)

Compound **11b**(white solid, 846 mg, 90 % yield) was prepared following the general synthetic procedure of compound **11a**.^{1}H NMR (500 MHz, DMSO-d_6) δ 12.58 (s, 1H), 7.97 (d, J = 8.4 Hz, 2H), 7.84 (d, J = 8.5 Hz, 2H), 7.64 (d, J = 16.1 Hz, 1H), 6.66 (d, J = 16.1 Hz, 1H), 3.86 (s, 3H).

4.2.33. Methyl (E)-3-(3-oxo-3-((trityloxy)amino)prop-1-en-1-yl)benzoate (12a)

Compound **12a** (white solid, 857 mg, 56 %) was prepared following the same synthetic procedure of compound **5a**. ^{1}H NMR (500 MHz, Chloroform-*d*) δ 7.97 (d, J = 7.3 Hz, 1H), 7.87 (s, 1H), 7.54–7.27 (m, 19H), 6.11 (d, J = 15.9 Hz, 1H), 3.93 (s, 3H).

4.2.34. Methyl (E)-4-(3-oxo-3-((trityloxy)amino)prop-1-en-1-yl)benzoate (12b)

Compound **12b** (white solid, 743 mg, 67 %) was prepared following the same synthetic procedure of compound **5a** ^{1}H NMR (500 MHz, Chloroform-*d*) δ 7.95 (d, J = 8.1 Hz, 2H), 7.53–7.24 (m, 17H), 6.15 (d, J = 15.9 Hz, 1H), 3.90 (s, 3H).

4.2.35. (E) -3-(3-oxo-3-((trityloxy)amino)prop-1-en-1-yl)benzoic acid (13a)

Compound **13a** (white solid, 752 mg, 88 %) was prepared following the same synthetic procedure of compound **6a**. ^{1}H NMR (500 MHz, DMSO-d_6) δ 13.11 (s, 1H), 10.45 (s, 1H), 7.89 (d, J = 7.7 Hz, 1H),7.59–7.46 (m, 3H), 7.41–7.22 (m, 15H), 6.57 (d, J = 15.9 Hz, 1H).

4.2.36. (F) -4-(3-oxo-3-((trityloxy)amino)prop-1-en-1-yl)benzoic acid (13b)

Compound **13b** (white solid, 967 mg, 93 %) was prepared following the same synthetic procedure of compound **6a**. ^{1}H NMR (500 MHz, DMSO-d_6) δ 13.01 (s, 1H), 10.51 (s, 1H), 7.91 (d, J = 8.1 Hz, 2H), 7.59 (d, J = 8.0 Hz, 2H), 7.41–7.22 (m, 15H), 6.61 (d, J = 15.9 Hz, 1H).

4.2.37. (3aR,4aR,6R,8aR,9aR)-8a-methyl-3,5-dimethylene-2-oxododecahydronaphtho[2,3-b]furan-6-yl(3-((E)-3-(hydroxyamino)-3-oxoprop-1-en-1-yl)benzoyl)glycinate (15)

Compound **15** (yellow solid, 25 mg, 49 %) was prepared following the same synthetic procedure of compound **12** ^{1}H NMR (500 MHz, DMSO-d_6) δ 10.84 (s, 1H), 9.09 (t, J = 6.0 Hz, 1H), 8.11 (s, 1H), 7.88 (d, J = 7.8 Hz, 1H), 7.74 (d, J = 7.7 Hz, 1H), 7.55 (t, J = 7.7 Hz, 1H), 7.50 (d, J = 15.8 Hz, 1H), 6.56 (d, J = 15.8 Hz, 1H), 5.95 (s, 1H), 5.71 (s, 1H), 5.29 (s, 1H), 5.09 (s, 1H), 4.68 (s, 1H), 4.35 (t, J = 4.8 Hz, 1H), 4.03 (d, J = 5.9 Hz, 2H), 2.85 (dd, J = 11.9, 6.0 Hz, 1H), 2.11 (d, J = 12.5 Hz, 1H), 1.94 (d, J = 15.4 Hz, 1H), 1.78–1.64 (m, 2H), 1.58 (ddd, J = 13.9, 7.2, 2.6 Hz, 1H), 1.50–1.40 (m, 1H), 1.30–1.18 (m, 2H), 1.16–1.04 (m, 1H), 0.68 (s, 3H).^{13}C NMR (125 MHz, DMSO) δ 169.88, 168.64, 166.38, 162.36, 145.53, 141.99, 137.51, 135.08, 134.31, 130.97, 129.28, 128.14, 125.86, 120.47, 120.25, 112.23, 76.14, 75.47, 41.86, 40.57, 35.45, 33.38, 26.61, 26.33, 16.77. HRMS(ESI) *m/z* calced for $C_{27}H_{31}N_2O_7$ [M+H]$^+$495.2126 , found 495.2128.

4.2.38. (3aR,4aR,6R,8aR,9aR)-8a-methyl-3,5-dimethylene-2-oxododecahydronaphtho[2,3-b]furan-6-yl(3-((E)-3-(hydroxyamino)-3-oxoprop-1-en-1-yl)benzoyl)-R-alaninate (16)

Compound **16** (yellow solid, 57 mg, 48 %) was prepared following the same synthetic procedure of compound **12** .^{1}H NMR (500 MHz, DMSO-d_6) δ 10.82 (s, 1H), 8.89 (d, J = 7.1 Hz, 1H), 8.13 (s, 1H), 7.91 (d, J = 7.8 Hz, 1H), 7.74 (d, J = 7.7 Hz, 1H), 7.55 (d, J = 7.7 Hz, 1H), 7.53–7.47 (m, 1H), 6.57 (d, J = 15.8 Hz, 1H), 5.95 (s, 1H), 5.72 (s, 1H), 5.25 (s, 1H), 5.07 (s, 1H), 4.66 (s, 1H), 4.52–4.42 (m, 1H), 4.36–4.30 (m, 1H), 2.85–2.77 (m,1H), 2.06 (d, J = 12.3 Hz, 1H), 1.92 (d, J = 14.7 Hz, 1H), 1.78–1.65 (m, 2H), 1.55 (ddd, J = 13.8, 7.1, 2.7 Hz, 1H), 1.50–1.44 (m, 1H), 1.42 (d, J = 7.4 Hz, 3H), 1.30–1.23 (m, 1H), 1.20–1.04 (m, 2H), 0.67 (s, 3H). ^{13}C NMR (125 MHz, DMSO) δ 171.38, 169.86, 165.99, 162.45, 145.54, 141.95, 137.54, 134.98, 134.33, 130.92, 129.14, 128.32, 125.97, 120.49, 120.19, 112.09, 76.10, 75.25, 48.84, 40.49, 35.53, 33.35, 26.60, 26.31, 16.73, 16.53. HRMS(ESI) *m/z* calced for $C_{28}H_{33}N_2O_7$ [M+H]$^+$509.2282 , found 509.2284.

4.2.39. (3aR,4aR,6R,8aR,9aR)-8a-methyl-3,5-dimethylene-2-oxododecahydronaphtho[2,3-b]furan-6-yl(3-((E)-3-(hydroxyamino)-3-oxoprop-1-en-1-yl)benzoyl)-S-alaninate (17)

Compound **17**(yellow solid, 22 mg, 46 %) was prepared following the same synthetic procedure of compound **12** .^{1}H NMR (500 MHz, DMSO-d_6) δ 10.85 (s, 1H), 8.89 (d, J = 7.3 Hz, 1H), 8.14 (s, 1H), 7.90 (d, J = 7.8 Hz, 1H), 7.74 (d, J = 7.6 Hz, 1H), 7.58–7.48 (m, 2H), 6.57 (d, J = 15.8 Hz, 1H), 5.94 (s, 1H), 5.65 (s, 1H), 5.25 (s, 1H), 5.10 (s, 1H), 4.67 (s, 1H), 4.53 (t, J = 7.3 Hz, 1H), 4.32–4.27 (m, 1H), 2.76–2.68 (m, 1H), 2.09 (d, J = 12.5 Hz, 1H), 1.91 (d, J = 14.7 Hz, 1H), 1.77–1.61 (m, 2H), 1.56 (ddd, J = 13.9, 7.0, 2.7 Hz, 1H), 1.43 (d, J = 7.3 Hz, 3H), 1.38 (dd, J = 13.3, 4.7 Hz, 1H), 1.28–1.20 (m, 1H), 1.17–1.04 (m, 2H), 0.67 (s, 3H).^{13}C NMR (125 MHz, DMSO) δ 171.32, 169.81, 166.00, 162.43, 145.53, 141.94, 137.57, 134.95, 134.39, 130.90, 129.19, 128.47, 125.95, 120.35, 120.20, 112.08, 76.07, 75.51, 48.66, 40.61, 35.38, 33.34, 26.50, 26.29, 16.74, 16.51. HRMS(ESI) *m/z* calced for $C_{28}H_{33}N_2O_7$ [M+H] $^+$509.2282, found 509.2284.

4.2.40. (3aR,4aR,6R,8aR,9aR)-8a-methyl-3,5-dimethylene-2-oxododecahydronaphtho[2,3-b]furan-6-yl(4-((E)-3-(hydroxyamino)-3-oxoprop-1-en-1-yl)benzoyl)-R-alaninate (18)

Compound **18** (yellow solid, 34 mg, 50 %) was prepared following the same synthetic procedure of compound **12**.^{1}H NMR (500 MHz, DMSO-d_6) δ 10.83 (s, 1H), 9.12 (s, 1H), 8.84 (d, J = 7.2 Hz, 1H), 7.95 (d, J = 8.0 Hz, 2H), 7.69 (d, J = 8.0 Hz, 2H), 7.50 (d, J = 15.8 Hz, 1H), 6.55 (d, J = 15.8 Hz, 1H), 5.96 (s, 1H), 5.74 (s, 1H), 5.25 (s, 1H), 5.07 (s, 1H), 4.66 (s, 1H), 4.46 (t, J = 7.2 Hz, 1H), 4.43–4.37 (m, 1H), 2.92–2.83 (m, 1H), 2.09 (d, J = 12.5 Hz, 1H), 1.94 (d, J = 15.0 Hz, 1H), 1.78–1.64 (m, 2H), 1.57 (ddd, J = 13.9, 7.1, 2.6 Hz, 1H), 1.52–1.42 (m, 1H), 1.41 (d, J = 7.3 Hz, 3H), 1.31–1.20 (m, 2H), 1.09 (q, J = 12.8 Hz, 1H), 0.68 (s, 3H).^{13}C NMR (125 MHz, DMSO) δ 171.41, 169.89, 165.80, 162.41, 145.57, 142.05, 137.84, 137.32, 134.15, 128.10, 127.39, 120.99, 120.45, 112.09, 76.17, 75.26, 48.77, 40.46, 35.57, 33.37, 26.61, 26.35, 16.75, 16.54.HRMS(ESI) *m/z* calced for $C_{28}H_{33}N_2O_7$ [M+H]$^+$509.2282, found 509.2279.

4.2.41. (3aR,4aR,6R,8aR,9aR)-8a-methyl-3,5-dimethylene-2-oxododecahydronaphtho[2,3-b]furan-6-yl(4-((E)-3-(hydroxyamino)-3-oxoprop-1-en-1-yl)benzoyl)-S-alaninate (19)

Compound **19** (yellow solid, 43 mg, 54 %) was prepared following the same synthetic procedure of compound **12**. ^{11}H NMR (500 MHz, DMSO-d_6) δ 10.83 (s, 1H), 8.84 (d, J = 7.3 Hz, 1H), 7.95 (d, J = 8.0 Hz, 2H), 7.69 (d, J = 8.0 Hz, 2H), 7.50 (d, J = 15.8 Hz, 1H), 6.55 (d, J = 15.9 Hz, 1H), 5.95 (s, 1H), 5.69 (s, 1H), 5.24 (s, 1H), 5.10 (s, 1H), 4.67 (s, 1H), 4.56–4.47 (m, 1H), 4.38 (t, J = 4.0 Hz, 1H), 2.80–2.72 (m , 1H), 2.11 (d, J = 12.4 Hz, 1H), 1.94 (d, J = 15.1 Hz, 1H), 1.77–1.62 (m, 2H), 1.56 (ddd, J = 13.9, 7.1, 2.6 Hz, 1H), 1.43 (d, J = 7.4 Hz, 3H), 1.41–1.37 (m, 1H), 1.31–1.23 (m, 2H), 1.16–1.04 (m, 1H), 0.68 (s, 3H).^{13}C NMR (125 MHz, DMSO) δ 171.36, 169.85, 165.79, 162.32, 145.56, 142.04, 137.89, 137.26, 134.17, 128.12, 127.39, 121.01, 120.34, 112.08, 76.16, 75.49, 48.61, 40.55, 35.42, 33.37, 26.52, 26.33, 16.76, 16.54. HRMS (ESI) *m/z* calced for $C_{28}H_{33}N_2O_7$ [M+H] $^+$509.2282, found 509.2286.

4.3. Cell viability assay

Cell viability was determined using the CCK-8 assay (Dojindo Laboratories, Japan). Briefly, cells were seeded into 96-well plate and allowed to adhere overnight. Cells were then treated with tested compounds for 72 h. Next, the cells were incubated with CCK8 dye at 37 °C for 1 h and the absorbance was determined at a wavelength of 450 nm using a microplate reader (Biotek NEO2).

4.4. In vitro HDAC inhibition assay

Recombinant human HDAC enzymes were purchased from BPS Bioscience. The histone deacetylase inhibitory activity of HDAC1, 2, 3, and 6 was assayed with substrate Boc-Lys (acetyl)-AMC while the inhibitory activity of HDAC 4, 5, 7, 8, 9, and 11 was determined using substrate Boc-Lys (trifluoroacetyl)-AMC. The HDAC enzyme was dissolved in 30 μL of buffer containing 25 mM Tris (pH 8.0), 1 mM $MgCl_2$, 0.1 mg/mL BSA, 137 mM NaCl, and 2.7 mM KCl, and incubated with tested compound at 37 °C for 1 h, then 20 μL of HDAC substrate was added. After incubation at 37 °C for 1 h, the reaction of was quenched with the addition of 40 μL developer solution containing 6 mg/mL trypsin and 33 μM trichostatin A. The plates were incubated for 30 min at room temperature, and the fluorescence signal was collected at 350 nm (excitation) and 450 nm (emission) by using a microplate reader.

4.5. SPR assay

Compounds bound to STAT protein were determined using Biacore 8K (GE Healthcare) system according to standard methods. STAT

protein (100 μg/mL) was dissolved in sodium acetate buffer (PH 4.5) and immobilized on a CM5 sensor chip using an amine coupling kit (GE Healthcare). The compounds were diluted with 5 % DMSO in PBS buffer. The equilibrium dissociation constant K_D was fitted by using the Biacore Insight Evaluation software.

4.6. Fluorescent polarization-based binding assay

Recombinant human STAT3 protein and **18** was incubated in the buffer containing 50 mM NaCl, 10 mM HEPES, pH 7.5, 2 mM Dithiothreitol, 1 mM EDTA, and 0.01 % Triton-X100. After 1 h, 10 nM fluorescent peptide 5-FAM-G(pTyr)LPQTV-NH_2 (Allpeptide) was added. After incubation at room temperature for 30 min, polarization values were determined in a microplate reader at excitation and emission wavelengths of 485 and 530 nm, respectively.

4.7. Western blotting analysis

A549 cells were cultured in 6-well plates and treated with tested compounds or vehicle (0.1 % DMSO). After 12 h, the cells were harvested with RIPA buffer. Cell lysates of equal amounts were denatured and separated on 10 % SDS-PAGE, and transferred to PVDF membranes (Millipore). Then the membranes were blocked with 5 % nonfat milk for 2 h. Subsequently, the membranes were incubated with primary antibodies overnight at 4 °C, followed with incubating by a secondary antibody. Finally, the immunoblots were visualized by enhanced chemiluminescence (Millipore). Proteins were detected following primary antibodies: STAT3 (CST), phos- STAT3 (CST), Bcl-2 (CST), Bax (CST), Cleaved Caspase3 (CST), Ac-H3 (CST), Ac-H4 (CST), Ac-α-Tubulin (CST), LC3 (CST), P62 (CST), and GAPDH (Proteintech).

4.8. Cellular thermal shift assay (CETSA)

A549 cells were seeded in a 15 cm dish and treated with 6 μM of **18** for 4 h. The cells were harvested and suspended in 1 mL of PBS (containing PMSF and phosphatase inhibitor cocktail) and then divided into 0.2 mL PCR tubes. Each tube was heated at the designated temperature (44 °C、47 °C、50 °C、53 °C) for 3 min. Next, the cells were lysed through three freeze and thaw cycles. The cell lysates were centrifuged at 20,000g for 20 min at 4 °C. Then, the supernatants were subsequently analyzed by Western blot.

4.9. Cell apoptosis assay

A549 cells were seeded into 6-well plates and incubated with tested compounds or vehicle (0.1 % DMSO) for 24 h. Subsequently, cells were harvested and resuspended in binding buffer. The cells were incubated with 5 μL of FITC annexin V and 5 μL of propidium iodide (PI) at room temperature for 15 min. Flow cytometry was performed using the CytoFLEX S (Beckman, USA).

4.10. Transfection and fluorescence microscopy

A549 cells were seeded into confocal dishes and transfected with 2 μg of mRFP-GFP-LC3B plasmid using PEI transfection reagent for 24 h, then incubated with the tested compounds for 24 h. Subsequently, cells on coverslips were washed with ice cold PBS and fixed with 4 % paraformaldehyde. Images were captured using a Zeiss LSM700 confocal system (Carl Zeiss Microimaging, Thornwood, NY, USA) under a 63 × oil immersion objective.

4.11. Synthesis and characterization of self-assembled nanoparticles

Compound **18** (4 mg) was dissolved in DMSO (1.0 mL) and added to deionized water (4.0 mL), stirring at room temperature for 30 min. Subsequently, the solution dialyzed against deionized water for 24 h (MWCO = 10000) to give **18** NPs. The processing method of Ce6-**18** NPs was similar to that for **18** NPs. Briefly, **18** (2 mg) and Ce6 (0.5 mg) were dissolved in DMSO (2.0 mL) and added dropwise into 4.0 mL of deionized water, stirring at room temperature for 30 min. The particle size, PDI, and ζ-potential of NPs were determined with a Nanotrac wave II instrument, and triplicate measurements for each sample were taken. Nanoparticles were negatively stained and scanned with a transmission electron microscope to examine the morphology.

4.12. Stability of nanoparticles

The stability of **18** NPs and Ce6-**18** NPs was studied by monitoring the particle size and PDI. The solution of the nanoparticles was stored at 4 °C for 14 days. At different day intervals (0, 1, 2, 3, 5, 7, and 14 days), the average size and PDI were determined. At the same time, the 18 NPs were incubated in PBS (pH 7.4) containing 10 % FBS at 37 °C for 72 h.

4.13. In vitro drug release studies

2 mL of **18** NPs (0.5 mg/mL) was dialyzed (MWCO = 1000) in 60 mL different release medium (pH 7.4, 5.0, pH 7.4 + 10 % FBS) at 37 °C. At set time points, 2 mL of external buffer solution was took out and analyzed using an ACQUITY UPLC H-Class system.

4.14. Cellular uptake

Cellular uptake behaviors of Ce6 and **18-**Ce6 NPs were assessed by CLSM and flow cytometry. For fluorescence imaging, A549 cells were seeded for 24 h and then incubated with **18-**Ce6 NPs (10 mg/L) or the equivalent concentration of Ce6 (2 mg/L) for 4 h. Afterward, the fluorescence of A549 cells was observed by CLSM (EX: 594 nm). For flow cytometry quantification, the cells were seeded into 6-well plates and also incubated with Ce6 or **18-**Ce6 NPs for 4 h. Subsequently, the cells were washed and harvested. Flow cytometry was performed using the CytoFLEX S (Beckman, USA).

4.15. Pharmacokinetics and biodistribution

The use of animals was approved by Institutional Animal Care and Use Committee of Wuyi University (NO. CN2023017), with confirm adherence to the National Institutes of Health Guide for the Care and Use of Laboratory Animals. Male Sprague-Dawley (SD) rats were purchased from Guangdong Medical Laboratory Animal Center (Guangzhou, China). For pharmacokinetic studies, SD rats (~200 g) were randomly divided into **18** NPs and free **18** groups (n = 3). The IAL, **18** NPs, and free **18** were intravenously injected via tail vein at a dose of 5 mg/kg. The blood samples (0.5 mL) were taken from the eye socket at the 5 min, 1 h, 4 h, 8 h, and 12 h after injection. The plasma was obtained by centrifugation at 3000 rpm for 10 min and stored at −20 °C. Afterward, 200 μL of plasma two times with 250 μL of acetonitrile and methanol mixture (1:1 v/v). The solvent solutions separated by centrifugation were pooled. The concentrations of **18** were further analyzed by LC MS/MS analysis.

To assess the tissue distribution of free **18** and **18** NPs, the A549 tumor-bearing mice were intravenously injected via tail vein with **18** and **18** NPs at a dose of 5 mg/kg (n = 4). Mice were sacrificed by cervical vertebra dislocation at 6 h after drug administration, and the heart, liver, spleen, lung, kidney and tumor were collected. **18** were extracted from the homogenate using 2 mL of dichloromethane and methanol (4:1, *v/v*). The organic phases were collected and were further analyzed by LC MS/MS analysis.

4.16. In vivo fluorescence imaging

A549 tumor-bearing mice were injected intravenously via tail vein with 100 μL of **18-**Ce6 NPs (2 mg/mL) or the equivalent concentration of

free Ce6 (0.4 mg/mL). The fluorescence distribution was monitored at 0.5, 1, 3, 6, 9, 12 and 24 h using an *in vivo* imaging system with appropriate wavelength (λ ex = 680 nm, λ em = 750 nm).

4.17. In vivo anticancer activity

Female BALB/c nu/nu mice at 6–8 weeks (SLAC Laboratory Animal Co., LTD, Shanghai, China) were s.c. implanted with 5×10^6 A549 cells in the right flank. When tumors reached about 100 mm^3, mice were randomized into control and treatment groups (n = 5). The treatment groups received the compound **18** (5 mg/kg, 2.5 mg/kg), **18** NPs (5 mg/kg), and SAHA (10 mg/kg) intravenously every 3 day for 18 days. The control group was treated with saline solution. The tumor size was measured every 3 days and body weight was monitored regularly. After 18 days, all mice were sacrificed and dissected to weigh the tumor tissues and to examine the internal organ injury. For western blotting analysis, the treatment groups received the compound **18** (5 mg/kg), **18** NPs (5 mg/kg), and SAHA (10 mg/kg) intravenously every 3 day for 9 days. The control group was treated with saline solution.

4.18. Histological analysis

After 18 days of treatment, all mice were euthanized and tumors, as well as major organs (heart, liver, spleen, lung, and kidney), were collected for histological analysis including hematoxylin and eosin (H&E) staining and terminal deoxynucleotidyl transferase-mediated deoxyuridine triphosphate nick-end labeling (TUNEL, Roche Diagnostic, Indianapolis, IN, USA) assay.

4.19. Statistical analysis

Results are shown as means ± standard deviations for the indicated number of independently performed experiments. The statistical significance of the differences in mean values were determined by Student's t-test or ANOVA. *P < 0.05 indicates statistical significance, **P < 0.01 indicates high significance, and ***P < 0.001 1 indicates remarkable significance.

4.20. Calculation of combination index

On the basis of the results of the CCK8 assay, CI values were calculated using CompuSyn software according to the Chou-Talay method [33].

CRediT authorship contribution statement

Hualong Mo: Writing – original draft, Methodology, Investigation, Conceptualization. **JieYing Liu:** Investigation. **Zhengxi Su:** Investigation. **Deng-Gao Zhao:** Supervision, Funding acquisition, Formal analysis, Conceptualization. **Yan-Yan Ma:** Project administration, Funding acquisition, Conceptualization. **Kun Zhang:** Resources. **Qi Wang:** Investigation. **Chun Fu:** Investigation. **Yao Wang:** Project administration. **Meiwan Chen:** Funding acquisition, Conceptualization. **Burong Hu:** Resources, Project administration, Formal analysis.

Declaration of competing interest

The authors declare that they have no known competing financial interests or personal relationships that could have appeared to influence the work reported in this paper.

Data availability

Data will be made available on request.

Acknowledgements

This work was supported by the Department of Education of Guangdong Province (No. 2022ZDZX4054), the Hong Kong–Macao Joint Research and Development Fund of Wuyi University (No. 2022WGALH08), and the Jiangmen Program for Innovative Research Team (No.2018630100180019806).

Appendix A. Supplementary data

Supplementary data to this article can be found online at https://doi.org/10.1016/j.ejmech.2024.116765.

References

[1] W. Chen, R. Zheng, P.D. Baade, S. Zhang, H. Zeng, F. Bray, A. Jemal, X.Q. Yu, J. He, Cancer statistics in China, 2015, Ca-Cancer J. Clin. 66 (2) (2016) 115–132.
[2] D.J. Newman, Natural products and drug discovery, Natal. sci. rev. 9 (11) (2022) nwac206.
[3] S.T. Asma, U. Acaroz, K. Imre, A. Morar, S.R.A. Shah, S.Z. Hussain, D. Arslan-Acaroz, H. Demirbas, Z. Hajrulai-Musliu, F.R. Istanbullugil, A. Soleimanzadeh, D. Morozov, K. Zhu, V. Herman, A. Ayad, C. Athanassiou, S. Ince, Natural products/bioactive compounds as a source of anticancer drugs, Cancers 14 (24) (2022).
[4] Z. Guo, The modification of natural products for medical use, Acta Pharm. Sin. B 7 (2) (2017) 119–136.
[5] C. Gao, P. Bhattarai, M. Chen, N. Zhang, S. Hameed, X. Yue, Z. Dai, Amphiphilic drug conjugates as nanomedicines for combined cancer therapy, Bioconjugate Chem. 29 (12) (2018) 3967–3981.
[6] Y. Wang, P. Yang, X. Zhao, D. Gao, N. Sun, Z. Tian, T. Ma, Z. Yang, Multifunctional cargo-free nanomedicine for cancer therapy, Int. J. Mol. Sci. 19 (10) (2018) 2963–2983.
[7] P. Ma, J. Chen, X. Bi, Z. Li, X. Gao, H. Li, H. Zhu, Y. Huang, J. Qi, Y. Zhang, Overcoming multidrug resistance through the GLUT1-mediated and enzyme-triggered mitochondrial targeting conjugate with redox-sensitive paclitaxel release, ACS Appl. Mater. Interfaces 10 (15) (2018) 12351–12363.
[8] S. Dong, J. He, Y. Sun, D. Li, L. Li, M. Zhang, P. Ni, Efficient click synthesis of a protonized and reduction-sensitive amphiphilic small-molecule prodrug containing camptothecin and gemcitabine for a drug self-delivery system, Mol. Pharm. 16 (9) (2019) 3770–3779.
[9] Y. Shen, E. Jin, B. Zhang, C.J. Murphy, M. Sui, J. Zhao, J. Wang, J. Tang, M. Fan, E. Van Kirk, W.J. Murdoch, Prodrugs forming high drug loading multifunctional nanocapsules for intracellular cancer drug delivery, J. Am. Chem. Soc. 132 (12) (2010) 4259–4265.
[10] L. Fan, B. Zhang, A. Xu, Z. Shen, Y. Guo, R. Zhao, H. Yao, J.W. Shao, Carrier-free, pure nanodrug formed by the self-assembly of an anticancer drug for cancer immune therapy, Mol. Pharm. 15 (6) (2018) 2466–2478.
[11] Y. Yang, S. Wang, P. Ma, Y. Jiang, K. Cheng, Y. Yu, N. Jiang, H. Miao, Q. Tang, F. Liu, Y. Zha, N. Li, Drug conjugate-based anticancer therapy - current status and perspectives, Cancer Lett. 552 (2023) 215969.
[12] M. Sun, Q. Qian, L. Shi, L. Xu, Q. Liu, L. Zhou, X. Zhu, J.-M. Yue, D. Yan, Amphiphilic drug-drug conjugate for cancer therapy with combination of chemotherapeutic and antiangiogenesis drugs, Sci. China Chem. 63 (1) (2019) 35–41.
[13] P. Huang, D. Wang, Y. Su, W. Huang, Y. Zhou, D. Cui, X. Zhu, D. Yan, Combination of small molecule prodrug and nanodrug delivery: amphiphilic drug-drug conjugate for cancer therapy, J. Am. Chem. Soc. 136 (33) (2014) 11748–11756.
[14] S. Xu, X. Zhu, W. Huang, Y. Zhou, D. Yan, Supramolecular cisplatin-vorinostat nanodrug for overcoming drug resistance in cancer synergistic therapy, J. Contr. Release 266 (2017) 36–46.
[15] L. Yang, J. Xu, Z. Xie, F. Song, X. Wang, R. Tang, Carrier-free prodrug nanoparticles based on dasatinib and cisplatin for efficient antitumor in vivo, Asian J. Pharm. Sci. 16 (6) (2021) 762–771.
[16] R.G. Fu, Y. Sun, W.B. Sheng, D.F. Liao, Designing multi-targeted agents: an emerging anticancer drug discovery paradigm, Eur. J. Med. Chem. 136 (2017) 195–211.
[17] X. Li, X. Li, F. Liu, S. Li, D. Shi, Rational multitargeted drug design strategy from the perspective of a medicinal chemist, J. Med. Chem. 64 (15) (2021) 10581–10605.
[18] K.J. Falkenberg, R.W. Johnstone, Histone deacetylases and their inhibitors in cancer, neurological diseases and immune disorders, Nat. Rev. Drug Discov. 13 (9) (2014) 673–691.
[19] H.M. Hesham, D.S. Lasheen, K.A.M. Abouzid, Chimeric HDAC inhibitors: comprehensive review on the HDAC-based strategies developed to combat cancer, Med. Res. Rev. 38 (6) (2018) 2058–2109.
[20] S. Valente, A. Mai, Small-molecule inhibitors of histone deacetylase for the treatment of cancer and non-cancer diseases: a patent review (2011 - 2013), Expert Opin. Ther. Pat. 24 (4) (2014) 401–415.
[21] T.C.S. Ho, A.H.Y. Chan, A. Ganesan, Thirty years of HDAC inhibitors: 2020 Insight and hindsight, J. Med. Chem. 63 (21) (2020) 12460–12484.
[22] M. Hanif, J. Arshad, J.W. Astin, Z. Rana, A. Zafar, S. Movassaghi, E. Leung, K. Patel, T. Sohnel, J. Reynisson, V. Sarojini, R.J. Rosengren, S.M.F. Jamieson, C.

G. Hartinger, A multitargeted approach: organorhodium anticancer agent based on vorinostat as a potent histone deacetylase inhibitor, Angew. Chem. 59 (34) (2020) 14609–14614.
[23] S. He, G. Dong, Y. Li, S. Wu, W. Wang, C. Sheng, Potent dual BET/HDAC inhibitors for efficient treatment of pancreatic cancer, Angew. Chem. Int. Ed. 59 (8) (2020) 3028–3032.
[24] T. Liu, Y. Wan, Y. Xiao, C. Xia, G. Duan, Dual-target inhibitors based on HDACs: novel antitumor agents for cancer therapy, J. Med. Chem. 63 (17) (2020) 8977–9002.
[25] W. Liu, Y. Liang, X. Si, Hydroxamic acid hybrids as the potential anticancer agents: an Overview, Eur. J. Med. Chem. 205 (2020) 112679.
[26] W. Ge, Z. Liu, Y. Sun, T. Wang, H. Guo, X. Chen, S. Li, M. Wang, Y. Chen, Y. Ding, Q. Zhang, Design and synthesis of parthenolide-SAHA hybrids for intervention of drug-resistant acute myeloid leukemia, Bioorg. Chem. 87 (2019) 699–713.
[27] H. Zeng, J. Qu, N. Jin, J. Xu, C. Lin, Y. Chen, X. Yang, X. He, S. Tang, X. Lan, X. Yang, Z. Chen, M. Huang, J. Ding, M. Geng, Feedback activation of leukemia inhibitory factor receptor limits response to histone deacetylase inhibitors in breast cancer, Cancer Cell 30 (3) (2016) 459–473.
[28] Y. Ren, S. Li, R. Zhu, C. Wan, D. Song, J. Zhu, G. Cai, S. Long, L. Kong, W. Yu, Discovery of STAT3 and histone deacetylase (HDAC) dual-pathway inhibitors for the treatment of solid cancer, J. Med. Chem. 64 (11) (2021) 7468–7482.
[29] W. Chen, P. Li, Y. Liu, Y. Yang, X. Ye, F. Zhang, H. Huang, Isoalantolactone induces apoptosis through ROS-mediated ER stress and inhibition of STAT3 in prostate cancer cells, J. Exp. Clin. Cancer Res. 37 (1) (2018) 309.
[30] G. Babaei, S. Gholizadeh-Ghaleh Aziz, M. Rajabi Bazl, M.H. Khadem Ansari, A comprehensive review of anticancer mechanisms of action of Alantolactone, Biomed. Pharmacother. 136 (2021) 111231.
[31] Y. Zhou, X. Liu, J. Xue, L. Liu, T. Liang, W. Li, X. Yang, X. Hou, H. Fang, Discovery of peptide boronate derivatives as histone deacetylase and proteasome dual inhibitors for overcoming bortezomib resistance of multiple myeloma, J. Med. Chem. 63 (9) (2020) 4701–4715.
[32] J. Mantaj, S.M. Rahman, B. Bokshi, C.M. Hasan, P.J. Jackson, R.B. Parsons, K. M. Rahman, E. Crispene, A cis-clerodane diterpene inhibits STAT3 dimerization in breast cancer cells, Org. Biomol. Chem. 13 (13) (2015) 3882–3886.
[33] T.C. Chou, Drug combination studies and their synergy quantification using the Chou-Talalay method, Cancer Res. 70 (2) (2010) 440–446.